Interference Mitigation Enabled Signal Detection in Diffusive Molecular Communications Systems with Molecular Type Spreading

Weidong Gao, *Student Member, IEEE*, and Lie-Liang Yang, *Fellow, IEEE*

***Abstract*—To accomplish complex tasks, several nano-machines may need to communicate via multiple-access channel with one access point, where information fusion is carried out. However, multiple-access Diffusive Molecular Communications (DMC) systems suffer from severe Multiple-Access Interference (MAI) and Inter-Symbol Interference (ISI), which should be effectively mitigated at receiver in order to achieve acceptable performance. Built on two fundamental single-user detection schemes, namely Threshold assisted Majority Vote Detection (TMVD) and Equal Gain Combination Detection (EGCD), we first propose three low-complexity interference cancellation schemes, which are the TMVD-assisted Iterative Interference Cancellation (TMVD-IIC), TMVD-based Minimum-Distance Decoding assisted Interference Cancellation (TMVD-MDDIC) and the EGCD-assisted N-order Iterative Interference Cancellation (EGCD-NIIC), for operation in the Molecular Type Spread assisted Molecular Shift Keying (MTS-MoSK) DMC systems. Then, following the principle of maximum likelihood detection, we propose a Simplified Approximate Maximum Likelihood (SAML) detection scheme. The error performance of the MTS-MoSK DMC systems employing respectively the considered detection schemes is comprehensively investigated and compared. Furthermore, the complexities of the detection schemes are analyzed and discussed in terms of the complexity-performance trade-off. Our studies and results show that, compared with the single-user TMVD and EGCD schemes, the proposed interference cancellation schemes are capable of mitigating efficiently the effect of MAI and enabling significant performance improvement at the slightly increased complexity.**

***Index Terms*—Diffusive molecular communications, molecular shift keying, molecular type spreading, multiple-access interference, interference cancellation, minimum-distance decoding, majority vote, equal gain combining, inter-symbol interference, error performance.**

I. Introduction

Following Moore's law, nano-machines have been becoming smaller and smaller. In practice, nano-machines may find different applications, especially, in biology and healthcare. In literature, there are many novel researches on the health monitor and disease treatment that rely on the implementation of nano-machines [1–3]. However, the manufacture capability of nano-machines puts constraints on the computation or tasks that a nano-machine is able to accomplish [4]. Due to this kind of constraints, Internet of Nano-Machines (IoNM) needs to be constructed to allow various nano-machines to cooperate via information exchange, so as to complete complex tasks. As an efficient communication technique for IoNM, Molecular Communication (MC) has a range of advantages, including energy saving, biocompatibility, small size, etc. [5–7]. Besides playing the communication role in IoNM, MC has also been integrated with sensing techniques for application in the Internet of Medical Things (IoMT) to monitor and detect infectious diseases like COVID-19 [8]. In [9], the mechanism of viral spreading in the form of aerosols based on macro-scale MC prototypes was provided. As an energy-efficient and naturally common way to convey particles, Diffusion-based Molecular Communication (DMC) constitutes one of the promising techniques for information exchange in IoMN/IoMT [10]. However, a big challenge in DMC-based systems is inter-symbol interference (ISI) resulted from the slow propagation process of free diffusion. Hence, in literature, a range of methods have been proposed to combat ISI in DMC. For instance, various information modulation schemes were designed to reduce ISI [11–13]. The low-complexity equalization techniques inspired by the conventional radio-based communications were studied with DMC to mitigate ISI [14–16]. Furthermore, some noncoherent schemes without relying on Channel State Information (CSI) for signal detection were proposed for ISI mitigation in DMC [17, 18].

However, to implement the IoNM supported by MC, there is another critical design issue, i.e., how to design a multiple-access MC (MAMC) scheme to allow multiple nano-machines transmit information simultaneously with high-efficiency. For example, in a molecular sensor network, because of limited storage space and computation capability of individual nano-sensors, the observations attained by individual sensors need to be sent to a processing center for fusion. In this network, it is highly challenging for the multiple nano-sensors to propagate their sensed information to the processing center, reliably and efficiently. Nonetheless, to our knowledge, MAMC has not received sufficient attention in the MC research communities.

By following the principles of multiple-access wireless communications, in literature, some multiple-access schemes have been considered in DMC. More specifically, Molecular Division Multiple-Access (MDMA) proposed in [19–25] straightforwardly allocates different types of molecules to different nano-machines for signal transmissions. In this way, simultaneous transmissions of different nano-machines can be implemented in one medium without interfering with each other. The authors of [26, 27] proposed the Molecular Code-Division Multiple-Access (MCDMA), which assigns individual nano-machines unique signature codes for them to simultaneously transmit with a common receiver, where the signature codes are used to distinguish the information sent by different nano-machines. In [28–30], Molecular Time-Division Multiple-Access (MTDMA) was introduced to support multiple nano-machines to communicate with a common

W. Gao and L.-L. Yang are with School of Electronics and Computer Science, University of Southampton, SO17 1BJ, UK. (E-mail: wg1y15, lly@ecs.soton.ac.uk, http://www-mobile.ecs.soton.ac.uk/lly).

The authors would like to acknowledge the financial support of the Engineering and Physical Sciences Research Council project EP/X01228X/1.

receiver. In MTDMA DMC systems, different time slots are assigned to different nano-machines for them to alternatively send information without experiencing severe inter-user interference. Furthermore, considering that the molecular concentration impulse received is very sensitive to transmission distance in DMC, [31] and [32] proposed the Molecular Space Division Multiple-Access (MSDMA), which distinguishes different nano-machines via their distances from the receiver.

Due to the diffusive properties of DMC, multiple-access DMC (MA-DMC) usually experiences various types of interference, especially, Multiple-Access Interference (MAI). Furthermore, due to the slow process of Brownian motion, interference, especially MAI, in MA-DMC systems is likely to be severe. Hence, the designs of multiple-access schemes and transceivers are highly important in mitigating the interference in MA-DMC systems. In literature, there are some works having proposed and investigated the detection schemes for MA-DMC systems [21, 26, 28, 32]. Specifically, considering the MCDMA with On-Off Keying (OOK) modulation, a chip-threshold-based detection scheme was developed in [26], where an adaptive threshold is set according to the concentration values measured with the previous chips around the receiver. For the MoTDMA with Molecular Shift Keying (MoSK) [28], the authors adopted the detection approach presented in [33], which is also a threshold-based detection scheme. As this MoTDMA scheme employs two types of molecules to transmit binary data, the detector uses the observation of one type of molecules as the decision variable, while the observation of the other type of molecules is used as the adaptive threshold for the decision-making in each signal interval. For the MSDMA systems in [32], the expected shapes of the received molecular pulses corresponding to all the possible transmission cases are estimated, which are then compared respectively with the observation samples to achieve Information detection. Finally, in [21], different types of molecules were straightforwardly exploited for distinguishing the transmissions by different nano-machines.

Inspired by the Fast Frequency-Hopping M-ary Frequency Shift Keying (FFH-MFSK) scheme [34, 35] in the conventional wireless communications, we have proposed a Molecular Type Spread assisted Molecular Shift Keying (MTS-MoSK) scheme to support MA-DMC in [36]. In this MTS-MoSK DMC scheme, different nano-machines are assigned with unique address codes, which are used to implement molecular type hopping at transmitter and assist signal detection at receiver. For signal detection, in [36], two low-complexity single-use detection schemes have been studied, which are the Threshold assisted Majority Vote Detector (TMVD) and Equal Gain Combining Detector (EGCD). In [37], a simple MAI erasure assisted EGCD scheme has been proposed, which can improve the detection performance of EGCD. All these detection schemes have low complexity. However, due to the severe interference existing in the MTS-MoSK systems, the MTS-MoSK systems with these detectors can only support a low number of nano-machines. Otherwise, the error performance of MTS-MoSK systems is very poor. To enable a MTS-MoSK system to simultaneously support a relatively high number of nano-machines while attaining practically meaningful reliability, in this paper, we focus on the MAI mitigation by proposing and comparing a range of interference mitigation schemes for the MTS-MoSK systems. Specifically, three MAI cancellation schemes are proposed, which are the Minimum-Distance Decoding based Interference Cancellation (MDDIC), TMVD-assisted Iterative Interference Cancellation (TMVD-IIC) and the EGCD-assisted N-order Iterative Interference Cancellation (EGCD-NIIC). We investigate their achievable performance and compare it with that obtained by the TMVD or EGCD. Furthermore, as another bench-marker, we propose a Simplified Approximate Maximum Likelihood (SAML) detection scheme, which has high complexity, to compare it with the interference cancellation assisted detection schemes. Furthermore, we demonstrate the impact of different parameters on the error performance of MTS-MoSK DMC systems. In particular, we show the effect of the thresholds in the TMVD-MDDIC and TMVD-IIC schemes, and the number of nano-machines participated in the interference cancellation in the EGCD-NIIC scheme. Additionally, we analyze the complexities of all the detection schemes considered and show their performance-complexity trade-off.

The novelties and contributions of the paper can be summarized as follows.

- MTS-MoSK assisted MA-DMC systems with various detection schemes are introduced, investigated and compared, to show the feasibility for supporting multiple-access communications in DMC environments.
- Four detection schemes having MAI mitigation capability are proposed, which are the TMVD-MDDIC, TMVD-IIC, EGCD-NIIC and SAML. Among these four detection schemes, the TMVD-MDDIC, TMVD-IIC and EGCD-NIIC detection schemes rely on interference cancellation to mitigate MAI, while the SAML implements information detection in the principle of maximum likelihood (ML).
- The performance of the MTS-MoSK assisted MA-DMC systems with respectively these detection schemes and the TMVD and EGCD, which are the single-user detectors without attempting MAI mitigation, is investigated and compared. The impact of the parameters related to system design, channel, and detection schemes on system performance is comprehensively studied. Furthermore, the complexities of the detection schemes are analyzed to show the trade-off between complexity and performance.

The remainder of this paper is organized as follows. Section II introduces the MTS-MoSK DMC system model. In Section III, the principles of three MAI mitigation schemes and of the SAML detection scheme are introduced. Performance results are demonstrated and discussed in Section IV. Finally, the main conclusions from research are summarized in Section V.

II. System Description

The framework of our MTS-MoSK DMC system is shown in Fig. 1, which was firstly introduced in [36]. The specific system structure and the procedure of operations are detailed in the following subsections.

A. Description of Transmitter and Channel Model

We assume that M types of information molecules are employed to support $K \leq M$ nano-machines to exchange

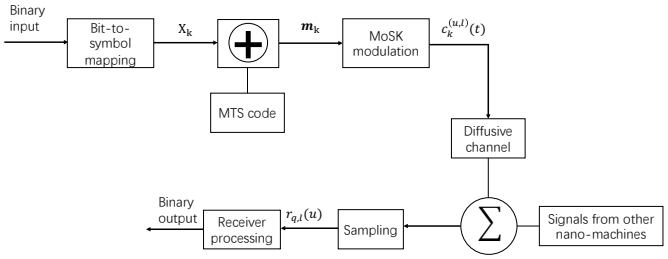

Fig. 1. System diagram demonstratiing the procedures of the MTS-MoSK DMC systems.

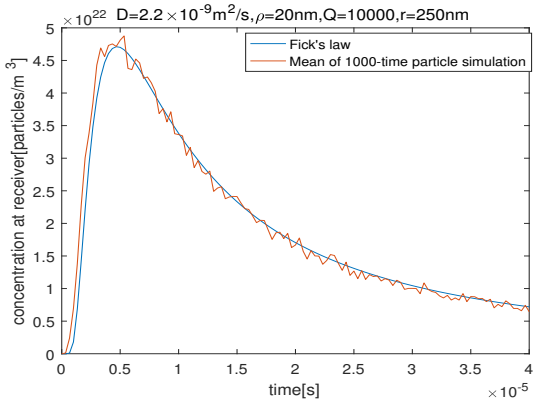

Fig. 2. Comparison between the expectation of concentration predicated by Fick's law of (2) and the average concentration obtained from 1000 particle-based simulations, when assuming that an impulse of 10000 molecules is emitted at $t = 0$.

information with a common access point (AP). The nano-machines and AP are static and their positions do not vary during a communication session. For simplicity, each nano-machine is assumed to have a similar distance from the AP. Note that, this can be a practical case in molecular sensor network (MSN). For example, several sensors monitoring an event may be arranged to have a similar distance from a fusion center, where the sensors upload their sensed data. In Fig. 1, the transmission of several bits of binary data from one nano-machine is demonstrated as the upper half of the figure. We assume that each nano-machine uses M types of molecules to transmit information in the form of M-ary symbols. Hence, each nano-machine can send $b = \log_2 M$ bits information per symbol. The symbol-duration is represented as T_s, which is divided into $L = T_s/T_h$ chips. Each chip takes up $T_h = T_s/L$ seconds, referred to as chip-duration. In our system model, we also assume that the K nano-machines implement synchronous transmission at chip level. In practice, AP can send periodic pilot signals to the nano-machines for them to synchronize their transmissions. As Fig. 1 shows, at the beginning of a T_s-second symbol-duration, b bits of binary data to be transmitted by the kth nano-machine is mapped to a M-ary symbol, which is expressed as $X_k \in \{0, 1, \ldots, M-1\}$. Then, the M-ary symbol X_k is signed by the molecular type spreading (MTS) code of the kth nano-machine. The kth nano-machine's MTS code can be expressed as $\boldsymbol{a}_k = [a_k^{(0)}, a_k^{(1)}, \ldots, a_k^{(L-1)}]$, $k = 1, 2, \ldots, K$, $a_k^{(i)} \in [0, M-1]$. The signature operation in Fig. 1 can be expressed as

$$\begin{aligned}\boldsymbol{m}_k =& [m_k^{(0)}, m_k^{(1)}, \ldots, m_k^{(L-1)}] \\ =& X_k \cdot \mathbf{1}_{(1\times L)} \oplus \boldsymbol{a}_k \\ =& [X_k \oplus a_k^{(0)}, X_k \oplus a_k^{(1)}, \ldots, X_k \oplus a_k^{(L-1)}], \\ & k = 1, 2, \ldots, K \end{aligned} \tag{1}$$

where $\mathbf{1}_{(1\times L)}$ is a row vector of L ones, which is used to extend the symbol X_k to a row vector with L elements of all being X_k, $\oplus$ is the addition operation in the Galois field GF (M) [38]. The elements of $\boldsymbol{m}_k$ are the symbols signed by the MTS code at chip scale and they are the integer values in $[0, M-1]$. After the signature operation, the MoSK modulation block in Fig. 1 controls the emission of the corresponding M types of molecules according to the values in $\boldsymbol{m}_k$ over the L chip-durations.

To explain the transmission process more clearly, let us assume a MTS-MoSK DMC system, which employs $M = 8$ types of molecules and $L = 6$ chips per symbol to support the information transmission of two nano-machines to an AP. Two MTS codes of $\boldsymbol{a}_1 = [4, 3, 7, 6, 2, 5]$ and $\boldsymbol{a}_2 = [2, 0, 1, 6, 4, 7]$ are assigned to the two nano-machines, respectively. Data symbols to be transmitted by two nano-machines are assumed to be $X_1 = 5$ and $X_2 = 3$. Then, X_1 and X_2 are extended to the L-length row vectors of $X_1 \cdot \mathbf{1}_{(1\times L)} = [5, 5, 5, 5, 5, 5]$ and $X_2 \cdot \mathbf{1}_{(1\times L)} = [3, 3, 3, 3, 3, 3]$, respectively. Then, these two row vectors execute the addition operation in Galois field $GF(8)$ with $\boldsymbol{a}_1$ and $\boldsymbol{a}_2$, yielding $\boldsymbol{m}_1 = X_1 \cdot \mathbf{1}_{(1\times L)} \oplus \boldsymbol{a}_1 = [1, 6, 2, 3, 7, 0]$ and $\boldsymbol{m}_2 = X_2 \cdot \mathbf{1}_{(1\times L)} \oplus \boldsymbol{a}_2 = [1, 3, 2, 5, 7, 4]$, respectively, where every element value corresponds to a type of molecules to be emitted within its chip-duration. Note that, the red elements in $\boldsymbol{m}_1$ and $\boldsymbol{m}_2$ indicate that the transmissions from two nano-machines generate collisions, which results in MAI, because the two nano-machines emit the same type of molecules during the same chip duration.

Assume that the MTS-MoSK DMC system employs the M types of isomer molecules, which have similar physical properties, including a similar diffusion coefficient expressed by D, when diffusing in a fluid medium [39]. After the MoSK modulation, a type of molecules are emitted at the beginning of a chip duration. Then, the concentration of this type of molecules around the receiver AP will start arising from the beginning of this chip-duration. We assume that within the lth chip duration of the uth symbol-duration, the qth type of molecules is activated for transmission by the kth nano-machine. According to Fick's second law [40, 41], the concentration observed at the AP varies with time t as

$$\begin{aligned} c_{k,q}^{(u,l)}(t) =& \frac{A}{[4\pi D\,(t - uT_s - lT_h)]^{3/2}} \\ & \times \exp\left(\frac{-r^2}{4D\,(t - uT_s - lT_h)}\right), \\ & t \geq (uL + l)\,T_h; u = 0, 1, \ldots; l = 0, 1, \ldots, L-1 \end{aligned} \tag{2}$$

where r is the transmission distance from the kth nano-machine to AP and A is the total number of molecules emitted per pulse.

Fig. 2 shows a molecular pulse of concentration generated, when an impulse of $A = 10000$ molecules is emitted at $t = 0$. The smooth curve is computed from (2) of Fick's diffusion law. The vibrating curve is the average concentration obtained from 1000 realizations. Explicitly, the estimated concentration

agrees well with the concentration predicted by Fick's law of (2). However, the estimated concentration slightly fluctuates around the theoretical expectation, which is because of the random noise generated by the Brownian motion of molecules and the limited 1000 realizations. Note that, according to [42], in DMC, we usually treat the expected concentration of (2) as the ideal signal, while the expected concentration plus the random noise generated by Brownian motion is the actual observation at receiver.

According to the properties of the free diffusion phenomenon, it can be easily deduced that there are three kinds of interference in the multiple access DMC systems, including the MTS-MoSK DMC system considered in this paper. First, as mentioned in many references [43, 44], the molecules of a given type generated for transmitting previous symbols may overlap with that for the later symbols, generating ISI. Second, the random Brownian motion of molecules results in background noise, which is also referred to as counting noise [45]. Third, as in the MTS-MoSK DMC system, when a desired nano-machine transmits the type-m molecules at a chip duration, the other nano-machines may also transmit this type of molecules at the same time, which interferes with the desired nano-machine. Furthermore, the mth type of molecules transmitted in the previous chip durations by the other nano-machines also interfere the desired nano-machine in the considered chip-duration. These kinds of interference resulted from the multiple nano-machines' transmissions are referred as MAI. Therefore, to achieve reliable communication in the multiple access DMC systems, the detection scheme must be carefully designed, so that the effect from the various kinds of interference can be minimized. In this paper, our focus is on the design of the effective interference cancellation schemes, which will be detailed in the forthcoming discourses.

B. Observations Obtained by Receiver

As Fig. 2 shows, when emitting an impulse of molecules at the beginning of a chip, the expected peak of concentration is an appropriate sampling point for the receiver at AP to obtain observations. From (2), we can derive that this peak point occurs at $t_d = r^2/(6D)$. Assume that in our MTS-MoSK DMC system, the chip-duration is sufficiently long, so that the extreme point happens within one chip-duration, i.e., $T_h > t_d$. Then, the sampled observation within the lth chip-duration of the uth symbol can be expressed as

$$\begin{aligned} r_{q,l}(u) =& r_q(t = uT_s + lT_h + t_d), \\ & l = 0, 1, \ldots, L-1;\ u = 0, 1, \ldots; \\ & q = 0, 1, \ldots, M-1 \end{aligned} \tag{3}$$

When the Brownian motion generated noise, ISI and MAI, as discussed previously, are taken into account, it can be shown that $r_{q,l}(u)$ can be expressed as

$$\begin{aligned} r_{q,l}(u) =& \sum_{k=1}^{K} \sum_{i=0}^{\min\{I, uL+l\}} \ell_{k,q}^{uL+l-i} c_{k,q}(iT_h + t_d) \\ & + n_q(uT_s + lT_h + t_d) \\ =& \sum_{k=1}^{K} \sum_{i=0}^{\min\{I, uL+l\}} \ell_{k,q}^{uL+l-i} c_{k,q}(i) + n_{q,l}(u) \end{aligned} \tag{4}$$

where I represents the ISI length in chip-durations, and $\ell_{k,q}^{i}$ makes a logical decision, equating to '1', when the kth nano-machine emits the type-q molecules to transmit information within the ith chip-duration, and otherwise, is '0'. In (4), $c_{k,q}(i)$, i.e., $c_{k,q}(iT_h + t_d)$, is the expected concentration of the type-q molecules sampled at $t = iT_h + t_d$, if this type of molecules was emitted at $t = 0$. It can be conceived from (4) that only the term with $i = 0$ contributes the desired observation for the current chip, while all the other terms with $i \neq 0$ impose interference. Finally, $n_{q,l}(u)$ in (4) represents the background noise resulted from the diffusion of the type-q molecules, which can be approximated as a Gaussian distribution [44], with the probability density function (PDF) expressed as

$$n_{q,l}(u) \sim \mathcal{N}\left(0, \frac{1}{V} \sum_{k=1}^{K} \sum_{i=0}^{\min\{I, uL+l\}} \ell_{k,q}^{uL+l-i} c_{k,q}(i)\right) \tag{5}$$

where V is the volume of the detection sphere that the AP uses for sensing information particles. As shown in (5), the variance of noise is depended on the amplitude of signal, which explains that noise is introduced whenever a signal is transmitted. The higher power of transmitted signal results in the higher power of noise.

III. Signal Detection and MAI cancellation in MTS-MoSK DMC Systems

According to the indexes shown in (3), it can be inferred that there are in total ML observations sampled by the receiver at AP in every symbol-duration. In order to describe the principles of the detection and MAI mitigation schemes, the observations in one symbol duration are arranged to form a matrix $\boldsymbol{R}_u$, expressed as

$$\boldsymbol{R}_u = \begin{bmatrix} r_{1,1}(u) & r_{1,2}(u) & \cdots & r_{1,l}(u) & \cdots & r_{1,L}(u) \\ r_{2,1}(u) & r_{2,2}(u) & \cdots & r_{2,l}(u) & \cdots & r_{2,L}(u) \\ \vdots & \vdots & \ddots & \vdots & \ddots & \vdots \\ r_{q,1}(u) & r_{q,2}(u) & \cdots & r_{q,l}(u) & \cdots & r_{q,L}(u) \\ \vdots & \vdots & \ddots & \vdots & \ddots & \vdots \\ r_{M,1}(u) & r_{M,2}(u) & \cdots & r_{M,l}(u) & \cdots & r_{M,L}(u) \end{bmatrix} \tag{6}$$

where M rows correspond to the M molecular types representing the M possibly transmitted symbols, and L columns correspond to the L chips of a symbol-duration. The (q, l)th element of $\boldsymbol{R}_u$ is $r_{q,l}(u)$ given by (4).

Having obtained the observation matrix $\boldsymbol{R}_u$, below we introduce two fundamental detection schemes and four MAI-mitigation enabled algorithms for signal detection in MTS-MoSK DMC systems. More specifically, the first one, inspired by a conventional single-user noncoherent detection scheme in radio communication [46], implements the threshold filtering before the majority vote assisted detection, which is named as TMVD. The second one is the proposed TMVD-MDDIC, which implements the minimum-distance decoding assisted interference cancellation followed by TMVD. The third one carries out the iterative interference cancellation after the fundamental TMVD, which is referred to as TMVD-IIC [47]. The forth one is the conventional equal-gain combining assisted detection (EGCD) [48], based on which the fifth one iteratively

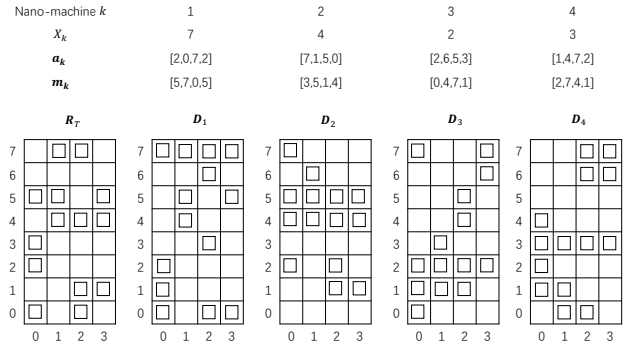

Fig. 3. An example to explain the TMVD for the MTS-MoSK DMC system supproting $K = 4$ nano-machines and employing $M = 8$ molecular types to transmit one symbol using $L = 4$ chips.

implements the EGCD and the N-order interference cancellation, which is referred to as NIIC-EGCD for convenience [49]. The last detection scheme is based on the ML principle, which is a common and optimum signal processing method in wireless communications.

A. Threshold-Assisted Majority Vote Detection

The detection principle of TMVD can be well explained using the example as shown in Fig. 3. In detail, the TMVD executes the following operations.

1) Based on the observation matrix $\boldsymbol{R}_u$, the TMVD inspects each of the elements against a preset threshold, which can be expressed as

$$T_h = \alpha c_h(0) \tag{7}$$

where $\alpha > 0$ is a scaling factor and $c_h(0)$ is the expected peak concentration, as shown in Fig. 2, which can be found from (2). The output of this procedure is a threshold-filtered matrix denoted by $\boldsymbol{R}_T$, as shown in Fig. 3, which contains the elements of '0' or '1', or 'empty' or 'mark'. Specifically, if an element in $\boldsymbol{R}_u$ is larger than T_h, the corresponding element in $\boldsymbol{R}_T$ is set to '1', representing that the element is marked. It is regarded as that this entry is activated by one or several nano-machines. By contrast, if an element in $\boldsymbol{R}_u$ is less than T_h, the corresponding element in $\boldsymbol{R}_T$ is set to '0', meaning that the receiver believes that no signal was transmitted by nano-machines in this entry.
2) The threshold-filtered matrix $\boldsymbol{R}_T$ is de-spread respectively by invoking the MTS signature codes of the K nano-machines, yielding K de-spread matrices, denoted by $\boldsymbol{D}_1, \boldsymbol{D}_2, \ldots, \boldsymbol{D}_K$. Specifically, based on the subtraction operation in the Galois field $GF(M)$, the (q, l) th element $r(q, l)$ in $\boldsymbol{R}_T$ is shifted to the location $(q \ominus a_k(l), l)$ in $\boldsymbol{D}_k$, i.e.,

$$d_{(k)}((q \ominus a_k(l), l)) = r(q, l),\ q = 0, 1, \ldots, M-1;\\ l = 0, 1, \ldots, L-1;\ k = 1, 2, \ldots, K \tag{8}$$

As shown in Fig. 3, after de-spreading, we obtain $\boldsymbol{D}_1, \boldsymbol{D}_2, \boldsymbol{D}_3$, and $\boldsymbol{D}_4$.
3) Finally, based on the de-spread matrices $\boldsymbol{D}_1, \boldsymbol{D}_2, \ldots, \boldsymbol{D}_K$, the decisions are made in the principle of majority votes, rendering the index of the row having the maximum number of 1s as the value of the transmitted symbol. Hence, with regard to the example shown in Fig. 3, the detected symbols are $\hat{X}_1 \in \{7\}$, $\hat{X}_2 \in \{4\ or\ 5\}$, $\hat{X}_3 \in \{2\}$, $\hat{X}_4 \in \{3\}$, respectively. As shown in Fig. 3 , $\boldsymbol{D}_1, \boldsymbol{D}_3$ and $\boldsymbol{D}_4$ each has just one majority row, which gives no confusive decision. By contrast, $\boldsymbol{D}_2$ has two majority rows, the TMVD has to choose randomly one of them as the detected symbol, which results in a symbol error probability of 0.5, even when the transmitted symbol was indeed 4 or 5.

Therefore, even when the channel is free of noise, TMVD may make erroneous detection because of the existence of the various interference as previously analyzed. In order to improve the detection performance, below we introduce the MAI-mitigation assisted detection schemes for MTS-MoSK DMC systems.

B. Minimum Distance Decoding Assisted Interference Cancellation (MDDIC)

The MDDIC algorithm is proposed to mitigate the interference experienced by TMVD by essentially examining the Hamming distance between the threshold-filtered observation matrix $\boldsymbol{R}_T$ and a range of constructed matrices based on the candidate symbols in detection. MDDIC is carried out after TMVD obtains the candidate symbols for the K nano-machines. In detail, MDDIC first lists all the possible combinations of the candidate symbols of the K nano-machines. Then, for each combination, the candidate symbols are spread by invoking the K nano-machines' MTS codes. In this way, a number of constructed matrices in the structure of $\boldsymbol{R}_T$ can be obtained. Finally, the similarity between any of these constructed matrices and the threshold-filtered observation matrix $\boldsymbol{R}_T$ is measured. On the basis of their Hamming distances, the combination giving the minimum distance from the threshold-filtered observation matrix $\boldsymbol{R}_T$ is selected, whose corresponding candidate symbols yield the finally detected symbols for the K nano-machines.

In detail, the principle of MDDIC can be understood with the aid of Fig 4 as follows.

1) TMVD as described in Section III-A is first carried out to generate the de-spread matrices $\boldsymbol{D}_1, \boldsymbol{D}_2, \boldsymbol{D}_3$ and $\boldsymbol{D}_4$, as shown in Fig 4. When only the full rows are considered, the candidate symbols are $\hat{X}_1 \in \{7\}$, $\hat{X}_2 \in \{4, 5\}$, $\hat{X}_3 \in \{2\}$ and $\hat{X}_4 \in \{3\}$. We can see that there are two candidate symbols for nano-machine 2.
2) All the combinations formed by the candidate symbols of K nano-machines are listed. For the example of Fig 4, the two combinations of candidate symbols are $\{\hat{X}_1 = 7,\ \hat{X}_2 = 4,\ \hat{X}_3 = 2,\ \hat{X}_4 = 3\}$ and $\{\hat{X}_1 = 7,\ \hat{X}_2 = 5,\ \hat{X}_3 = 2,\ \hat{X}_4 = 3\}$. Then, for each combination, the candidate symbols are respectively spread by invoking the corresponding MTS codes of the $K = 4$ nano-machines. As shown in Fig 4, after spreading the symbol of $\{\hat{X}_1 = 7,\ \hat{X}_2 = 4,\ \hat{X}_3 = 2,\ \hat{X}_4 = 3\}$, we obtain the matrices $\{\boldsymbol{E}_{11}, \boldsymbol{E}_{12}, \boldsymbol{E}_{13}, \boldsymbol{E}_{14}\}$. Similarly, for the combination $\{\hat{X}_1 = 7, \hat{X}_2 = 5, \hat{X}_3 = 2, \hat{X}_4 = 3\}$, we have $\{\boldsymbol{E}_{21}, \boldsymbol{E}_{22}, \boldsymbol{E}_{23}, \boldsymbol{E}_{24}\}$.
3) For each of the combinations, a matrix similar to $\boldsymbol{R}_T$ is constructed by adding the spreading matrices using the logical OR addition, forming the constructed observation matrix $\{\boldsymbol{F}_n\}$ for the n-th combination. As shown in Fig 4,

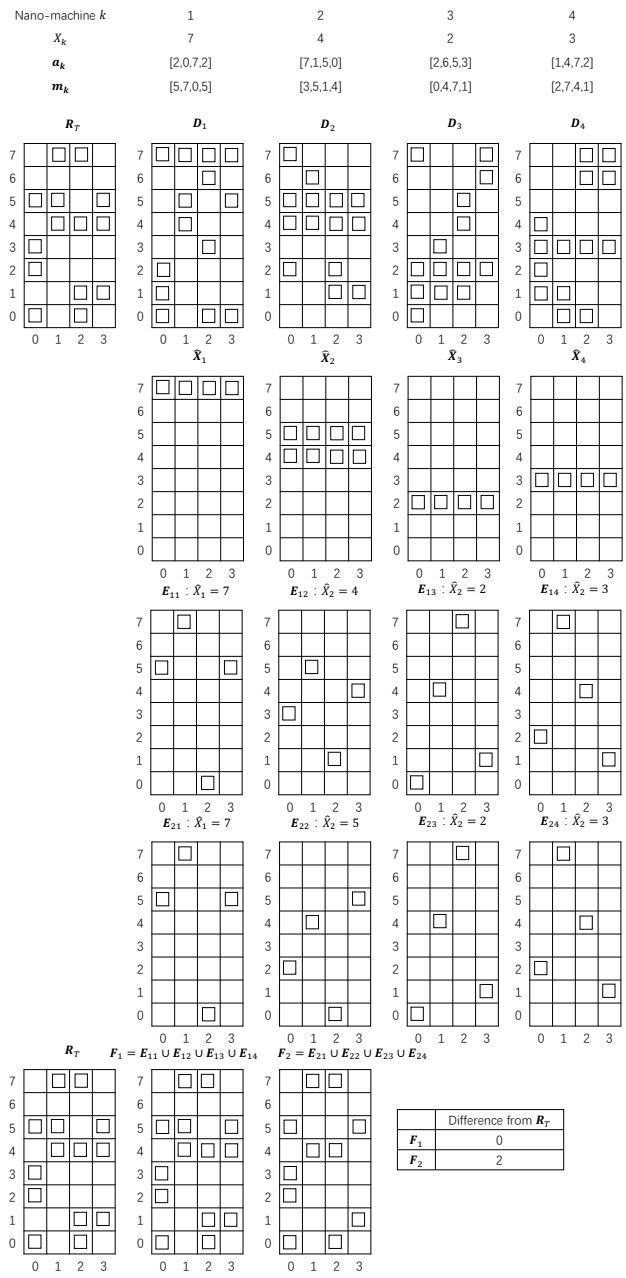

Fig. 4. Illustration of the TMVD-MDDIC for the MTS-MoSK DMC systems.

we have $\boldsymbol{F}_1 = \boldsymbol{E}_{11} \cup \boldsymbol{E}_{12} \cup \boldsymbol{E}_{13} \cup \boldsymbol{E}_{14}$ and $\boldsymbol{F}_2 = \boldsymbol{E}_{21} \cup \boldsymbol{E}_{22} \cup \boldsymbol{E}_{23} \cup \boldsymbol{E}_{24}$.

4) The final step of MDDIC is to compare the constructed observation matrices $\{\boldsymbol{F}_n\}$ with the threshold-filtered observation matrix $\boldsymbol{R_T}$ to select the combination yielding the minimum Hamming distance from $\boldsymbol{R}_T$. Correspondingly, the candidate symbols included in the selected combination represent the final decisions for the K symbols of the K nano-machines. Specifically for the example in Fig 4, we find that the distance between $\boldsymbol{F}_1$ and $\boldsymbol{R}_T$ is 0, while that between $\boldsymbol{F}_2$ and $\boldsymbol{R}_T$ is 2. Therefore, the first combination is finally selected, which gives the correctly detected symbols $\hat{X}_1 = 7$, $\hat{X}_2 = 4$, $\hat{X}_3 = 2$, $\hat{X}_4 = 3$.

In summary, the algorithm of TMVD-MDDIC is stated in Algorithm 1.

Algorithm 1 Minimum Distance Decoding assisted Interference Cancellation (MDDIC)

Input: Observation matrix $\boldsymbol{R}_u$.

Output: Symbols transmitted by K nano-machines within the uth symbol duration, expressed as $\hat{\boldsymbol{X}}(u)$.

1) **TMVD:** Execute TMVD as stated in Section III-A based on $\boldsymbol{R}_u$ to generate the threshold-filtered matrix $\boldsymbol{R}_T$ and the de-spread matrices $\{\boldsymbol{D}_k\}$. The row indices of each de-spread matrix $\boldsymbol{D}_k$ with the maximum number of activated entries are classified as the candidate symbols. The candidate symbols of kth nano-machine are collected to $\hat{\boldsymbol{X}}_k$.
2) **Combinations of candidate symbols:** Pick one element from each nano-machine's candidate symbol set $\hat{\boldsymbol{X}}_k$ to form all the possible combinations expressed as $\boldsymbol{P}_1, \boldsymbol{P}_2, \ldots, \boldsymbol{P}_n, \ldots, \boldsymbol{P}_N$, where N is the number of possible combinations and $\boldsymbol{P}_n = \{\hat{X}_{n1}, \hat{X}_{n2}, \ldots, \hat{X}_{nK}\}$.
3) **MDDIC:**
   For $i = 1, 2, \ldots, N$, execute the following steps:
   a) **Initialization:** The matrices $\boldsymbol{E}_{ik}$ are set as $(M \times L)$ all zero matrices.
   b) The candidate symbols of a combination $\boldsymbol{P}_i$ are respectively re-spread by invoking the corresponding MTS codes and then stored into the matrices $\boldsymbol{E}_{ik}$. The operation can be expressed as $e_{ik}\left(\hat{X}_{1k} \oplus a_k(l), l\right) = 1$, where $e_{ik}(m, l)$ is the (m, l)th element in $\boldsymbol{E}_{ik}$.
   c) $\boldsymbol{E}_{ik}$ are added based on the logical OR addition, giving $\boldsymbol{F}_i = \boldsymbol{E}_{i1} \cup \boldsymbol{E}_{i2} \cup \ldots \cup \boldsymbol{E}_{iK}$.
   d) Find the Hamming distance between $\boldsymbol{R}_T$ and $\boldsymbol{F}_i$ as $H_i = L_0(\boldsymbol{R}_T - \boldsymbol{F}_i)$, where $L_0(\boldsymbol{A})$ returns the number of nonzero elements of $\boldsymbol{A}$.
   End For
4) Find the $\boldsymbol{P}_n$ yielding the minimum Hamming distance, which is expressed as $n = \arg\min_n\{H_1, H_2, \ldots, H_N\}$.
5) **Output:** $\hat{\boldsymbol{X}}(u) = \boldsymbol{P}_n$.

It can be inferred from above that MDDIC is efficient to cancel MAI and improve the detection performance. More performance improvement is possible when more candidate symbols are tested. However, the computation and complexity may become dramatically high, when the number of candidate symbols is big and when the number of nano-machines supported is high.

C. TMVD-based Iterative Interference Cancellation (TMVD-IIC)

Since the MDDIC-assisted detector demands a high computation, when a MTS-MoSK system supports a large number of nano-machines, an IIC algorithm is proposed based on TMVD, so as to attain a good trade-off between complexity and reliability. This detector is referred to as the TMVD-IIC. Its operation principle is detailed as Algorithm 2 associated with the explanation as follow.

The principle of the TMVD-IIC can be explained with the aid of the example shown in Fig. 5. As Fig. 5 demonstrates, after the initial stage of TMVD, the transmitted symbols of three nano-machines, namely $k = 1, 3, 4$, can be detected as $\hat{X}_1 = 7$, $\hat{X}_3 = 2$ and $\hat{X}_4 = 3$, because their de-spread

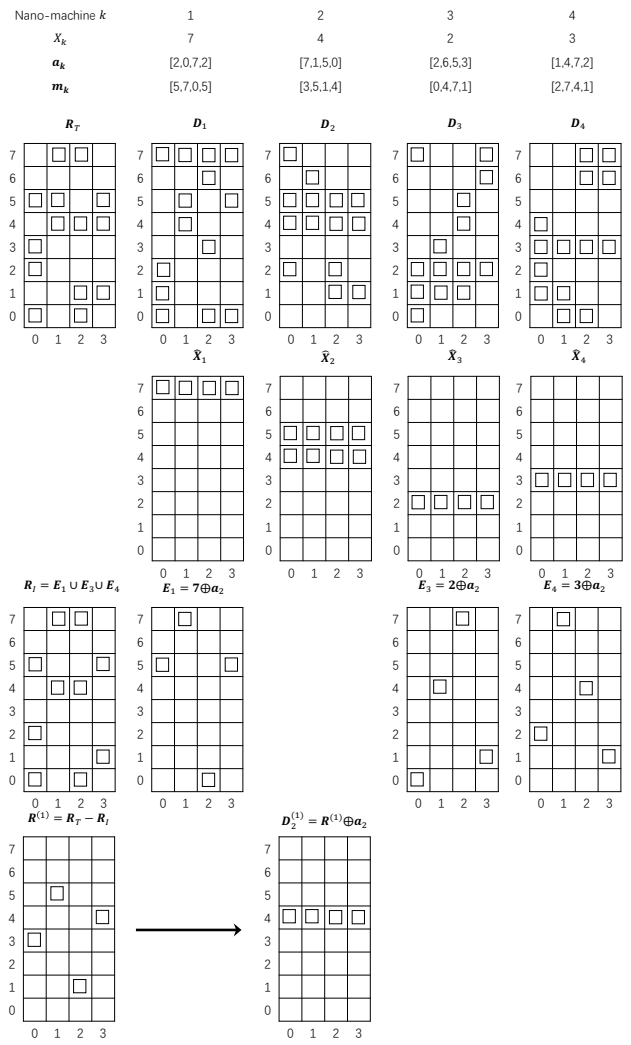

Fig. 5. Example to illustrate the operations of TMVD-IIC.

matrices $\boldsymbol{D}_1, \boldsymbol{D}_3, \boldsymbol{D}_4$ all have only one majority row. By contrast, the 2nd nano-machine has two candidate symbols $\{4, 5\}$. Therefore, during the IIC stage, the three re-spreading matrices of the nano-machines 1, 3 and 4, namely $\boldsymbol{E}_1, \boldsymbol{E}_3, \boldsymbol{E}_4$, are added in logical OR, yielding the interference matrix $\boldsymbol{R}_I$. Then, according to the interference matrix $\boldsymbol{R}_I$, the received matrix $\boldsymbol{R}_T$ is updated to $\boldsymbol{R}^{(1)}$ by operating the interference cancellation, which removes the elements in $\boldsymbol{R}_T$ according to the marked elements in $\boldsymbol{R}_I$. Finally, the detector de-spreads the updated matrix $\boldsymbol{R}^{(1)}$ using the 2nd nano-machine's MTS code $\boldsymbol{a}_2 = [7, 1, 5, 0]$, yielding the new de-spread matrix $\boldsymbol{D}_2^{(1)}$. Based on $\boldsymbol{D}_2^{(1)}$, the symbol transmitted by the 2nd nano-machine can be detected, which is $\hat{X}_2 = 4$, yielding the correct detection.

From the above description, we can infer that the TMVD-IIC algorithm is capable of improving the error performance of TMVD. It can be shown that the complexity of TMVD-IIC only increases linearly with the number of nano-machines supported.

Algorithm 2 TMVD-based Iterative Interference Cancellation (TMVD-IIC)

Input: Observation matrix $\boldsymbol{R}_u$.

Output: Symbols transmitted by K nano-machines within the uth symbol duration $\hat{\boldsymbol{X}}(u)$.

1) Execute TMVD to generate the de-spread matrices $\boldsymbol{D}_1, \ldots, \boldsymbol{D}_K$ corresponding to the individual nano-machines. In each of the de-spread matrices, the rows with the maximum number of entries are identified, whose indices represent the candidate symbols.
2) **If** a detection matrix contains only one majority row, the detector directly makes the decision to provide an estimate to the transmitted symbol in the principle of TMVD.
   Else: If detection matrix contains more than one majority row, the decision on the transmitted symbol is delayed to the later stages of the IIC, as explained below.
3) **Initialization:** $\boldsymbol{R}^{(0)} = \boldsymbol{R_T}$.
4) **For** $j = 1, 2, \ldots$, execute:
   a) The symbols detected by the nano-machines unambiguously at the $(j-1)$th iteration are respectively spreaded using the MTS codes of the nano-machines to form the re-spreading matrices.
   b) These re-spreading matrices are added element-by-element in logical OR to generate an interference matrix $\boldsymbol{R}_I$.
   c) The received matrix $\boldsymbol{R}^{(j-1)}$ is then updated to $\boldsymbol{R}^{(j)}$ by erasing the elements in $\boldsymbol{R}^{(j-1)}$ that have the same locations as those non-empty elements in the interference matrix $\boldsymbol{R}_I$.
   d) For each of the nano-machines whose transmitted symbols have not been detected, a new de-spread matrix as $\boldsymbol{D}_k^{(j)}$ is formed by de-spreading the updated matrix $\boldsymbol{R}^{(j)}$ using the nano-machine's MTS code. The majority rows of these de-spread matrices are then identified.
   If there are detection matrices without ambiguous rows, the decisions are made to provide the detected symbols.
   Else if there are no further symbols detected at the jth iteration or the maximum number of iterations is reached, randomly select a row as the detected symbol. Then, iteration **Stops**.
   Else: the detections for those nano-machines with ambiguous rows are left to the $(j+1)$th iteration.

End For

D. Equal-Gain Combining Detection (EGCD)

When the EGCD is employed, the detector first carries out de-spreading on $\boldsymbol{R}_u$ in the context of each nano-machine, generating the de-spread matrix $\boldsymbol{D}_{k,u}$ for the kth nano-machine. Specifically, the de-spreading process shifts the elements in $\boldsymbol{R}_u$ according to the rule of

$$d^{(k)}_{(q \ominus a_k(l), l)}(u) = r_{q,l}(u),\ q = 0, 1, \ldots, M-1;\\ l = 0, 1, \ldots, L-1;\ k = 1, 2, \ldots, K \quad (9)$$

where $\ominus$ represents the subtraction in $GF(M)$. Eq.(9) means that, after the de-spreading, the (q, l)th element $r_{q,l}(u)$ in $\boldsymbol{R}_u$

is shifted to the location of $(q \ominus a_k(l), l)$ in $\boldsymbol{D}_{k,u}$.

Based on the de-spread matrix $\boldsymbol{D}_{k,u}$, the detector executes the equal-gain combining (EGC) to form M decision variables for the kth nano-machine as

$$Z_q^{(k)}(u) = \sum_{l=0}^{L-1} d_{(q,l)}^{(k)}(u), \ q = 0, 1, \ldots, M-1; \quad k = 1, 2, \ldots, K \tag{10}$$

Finally, the largest decision variable in $\{Z_0^{(k)}(u), Z_1^{(k)}(u), \ldots, Z_{M-1}^{(k)}(u)\}$ is selected and its subscript represents the estimate to the symbol transmitted by the kth nano-machine. This decision making can be expressed as

$$\hat{X}_k(u) = \arg\max_q \{Z_q^{(k)}(u)\}, \ k = 1, 2, \ldots, K \tag{11}$$

When there is severe MAI in the MTS-MoSK DMC system, the EGCD's performance may be poor. In this case, MAI mitigation technique may be introduced to enhance the performance at relatively practical complexity. Let us now consider a NIIC algorithm for the purpose.

E. EGCD-assisted N-order Iterative Interference Cancellation (EGCD-NIIC)

EGCD-NIIC tries to detect the transmitted symbols of K nano-machines in the order from the most reliable one to the least reliable one by carrying out EGCD and NIIC iteratively. Once a symbol of a nano-machine is detected, the detector attempts to remove its effect on the following detections via interference cancellation. Hence, in EGCD-NIIC, efficiently measuring the reliabilities of the symbols to be detected is critical. In this paper, a simple but efficient reliability measurement approach is introduced by making use of the decision variables in $\boldsymbol{Z}^{(k)} = \left\{Z_0^{(k)}(u), Z_1^{(k)}(u), \ldots, Z_{M-1}^{(k)}(u)\right\}$ obtained by EGCD, which can be expressed as [50]

$$E^{(k)} = \frac{\max_2\{\boldsymbol{Z}^{(k)}\}}{\max_1\{\boldsymbol{Z}^{(k)}\}}, \ k = 1, 2, \ldots, K \tag{12}$$

where $\max_1\{\boldsymbol{Z}^{(k)}\}$ chooses the maximum of the decision variables in $\{Z_0^{(k)}(u), Z_1^{(k)}(u), \ldots, Z_{M-1}^{(k)}(u)\}$, while $\max_2\{\boldsymbol{Z}^{(k)}\}$ selects the second maximum from them. The nano-machine with a lower value of $E^{(k)}$ is rendered to be more reliable, as the result that the decision variable matching to the transmitted symbol has a significant difference from the other decision variables not matching to the transmitted symbol.

In detail, the EGCD-NIIC detector can be described as Algorithm 3.

From Algorithm 3 we know that EGCD-NIIC algorithm only attempts to mitigate the interference imposed by the first N most reliable nano-machines, while the symbols transmitted by the other nano-machines are detected by the conventional EGCD. Note that, for given values of K, L, signal-to-noise ratio, transmission distance r and data rate $1/T_b$, there is an optimal value for N to result in the best error performance, as shown by our performance results in Section IV.

Algorithm 3 EGCD-assisted N-order Iterative Interference Cancellation (EGCD-NIIC)

Input: Observation matrix $\boldsymbol{R}_u$, Number of iterations: N $(N < K)$.
Output: Detected symbols transmitted by K nano-machines within the uth symbol duration $\hat{\boldsymbol{X}}(u)$.
Initialization: $\boldsymbol{R}^{(0)} = \boldsymbol{R}_u$.
For $j = 1, 2, \ldots, N$, execute:

1) Corresponding to the $(K - j + 1)$ undetected nano-machines, their de-spread matrices $\boldsymbol{D}_j^{(1)}, \boldsymbol{D}_j^{(2)}, \ldots, \boldsymbol{D}_j^{(K-j+1)}$ are generated by applying their MTS codes, as done in (9).
2) Apply the EGC rule to these de-spread matrices, as shown in (10), yielding the M-length decision variable vectors $\boldsymbol{Z}^{(1)}, \boldsymbol{Z}^{(2)}, \ldots, \boldsymbol{Z}^{(K-j+1)}$.
3) Using (12) to measure the reliabilities for detecting these nano-machines, yielding $E_j^{(1)}, E_j^{(2)}, \ldots, E_j^{(K-j+1)}$.
4) Find the most reliable nano-machine from the $(K-j+1)$ undetected nano-machines, expressed as
$$\tilde{k} = \arg\min_k \{E_j^{(1)}, E_j^{(2)}, \ldots, E_j^{(k)}, \ldots, E_j^{(K-j+1)}\}$$
5) The symbol transmitted by the most reliable nano-machine $\tilde{k}$ is detected as the index of the maximum decision variable in $\boldsymbol{Z}^{(\tilde{k})}$. The detected symbol is expressed as $\hat{X}^{\tilde{k}}$.
6) Interference cancellation: the detector erases the $(\hat{X}^{\tilde{k}} \oplus a_{\tilde{k}}(l), l)$th, $l = 1, 2, \ldots, L$, elements in $\boldsymbol{R}^{(j-1)}$ to update $\boldsymbol{R}^{(j-1)}$ to $\boldsymbol{R}^{(j)}$, if these elements in $\boldsymbol{R}^{(j-1)}$ are not empty.

End For
Completion: Symbols transmitted by the remaining $K - N$ nano-machines are detected using $\boldsymbol{R}^{(N+1)}$ based on the conventional EGCD, as introduced in Section III-D. Then, detection **Stops**.

F. Simplified Approximate Maximum Likelihood Detection

In the MTS-MoSK DMC systems with ISI, the optimum detector is a sequential detector. Let us assume a MTS-MoSK DMC system with the ISI being $(I + 1)$ length. Then, the detection of the uth $(u > I)$ symbol depends on the former IK transmitted symbols. As the MTS-MoSK DMC system employs MoSK modulation, there are in total M^{IK} transmission states affecting the current symbol's detection. Hence, when the optimum Maximum Likelihood (ML) detection is employed, the detection complexity should be extremely high. To reduce the complexity, a simplified approximate ML (SAML) detector is proposed to detect the symbols of K nano-machines. In our SAML detection, the previously detected symbols are assumed to be correct, which reduces the detection complexity from $O\left(M^{IK}\right)$ to $O\left(M^K\right)$, which is explicitly only suitable for the system with a small K value.

The SAML detector estimates the K symbols transmitted by the K nano-machines during the uth symbol duration by maximizing the joint probability density function (pdf) of the K candidate symbols and the received signal samples, which

can be expressed as

$$\hat{\boldsymbol{X}}(u) = \arg\max_{\boldsymbol{X}(u)} f(\boldsymbol{R}_u, \boldsymbol{X}(u)) \tag{13}$$

where $\boldsymbol{R}_u$ is the observation matrix of (6) and $\boldsymbol{X}(u)$ represents the set of K candidate symbols of the K nano-machines possibly transmitted during the uth symbol duration. Upon applying the Bayes rule, and the fact that the symbols transmitted by different nano-machines are independent, we have

$$\begin{aligned} f(\boldsymbol{R}_u, \boldsymbol{X}(u)) =& P(\boldsymbol{X}(u)) f(\boldsymbol{R}_u \big| \boldsymbol{X}(u)) \\ =& \prod_{k=1}^{K} P(X_k(u)) \prod_{q=1}^{M} \prod_{l=1}^{L} f(r_{q,l}(u) \big| \boldsymbol{X}(u)) \end{aligned} \tag{14}$$

where the observations of the different types and of the different chips are also independent, when $\boldsymbol{X}(u)$ is given.

To maximize the joint pdf of (14), it is usually more convenient to minimize the negative logarithm of it. Thus, the SAML detector of Eq.(13) can be converted to

$$\begin{aligned} \hat{\boldsymbol{X}}(u) =& -\arg\min_{\boldsymbol{X}(u)} \ln \left[\prod_{k=1}^{K} P(X_k(u)) \prod_{q=0}^{M-1} \prod_{l=0}^{L-1} f(r_{q,l}(u) \big| \boldsymbol{X}(u)) \right] \\ =& -\arg\min_{\boldsymbol{X}(u)} \left[\sum_{k=1}^{K} \ln P(X_k(u)) + \sum_{q=0}^{M-1} \sum_{l=0}^{L-1} \ln f(r_{q,l}(u) \big| \boldsymbol{X}(u)) \right] \end{aligned} \tag{15}$$

Furthermore, if the probability of each transmitted symbol is the same, i.e., $P(X_k(u)) = 1/M$, the first term in the bracket of (15) is common and can be removed. Therefore, only the conditional pdf (the second term) in (15) needs to be minimized. Consequently, the SAML detector can be described as

$$\hat{\boldsymbol{X}}(u) = -\arg\min_{\boldsymbol{X}(u)} \sum_{q=0}^{M-1} \sum_{l=0}^{L-1} \ln f(r_{q,l}(u) \big| \boldsymbol{X}(u)) \tag{16}$$

From (4) and (5), we can know that $r_{q,l}(u)$ follows the Gaussian distribution expressed as

$$r_{q,l}(u) \sim \mathcal{N}\left(\mu_{q,l}(u), \sigma^2_{q,l}(u)\right) \tag{17}$$

where the mean and variance are

$$\begin{aligned} \mu_{q,l}(u) =& \sum_{k=1}^{K} \sum_{i=0}^{\min\{I, uL+l\}} \ell_{k,q}^{uL+l-i} c_{k,q}(i); \\ \sigma^2_{q,l}(u) =& \frac{1}{V} \mu_{q,l}(u) \end{aligned} \tag{18}$$

Explicitly, the pdf of $r_{q,l}(u)$ on the condition of $\boldsymbol{X}(u)$ can be expressed as

$$f(r_{q,l}(u) \big| \boldsymbol{X}(u)) = \frac{1}{\sqrt{2\pi\sigma^2_{q,l}(u)}} \exp\left[-\frac{(r_{q,l}(u) - \mu_{q,l}(u))^2}{2\sigma^2_{q,l}(u)} \right] \tag{19}$$

Substituting this pdf into the objective function of (16), we obtain

$$\begin{aligned} \Lambda^{ML}(\boldsymbol{R}_u, \boldsymbol{X}(u)) =& -\sum_{q=0}^{M-1} \sum_{l=0}^{L-1} \ln f(r_{q,l}(u) \big| \boldsymbol{X}(u)) \\ =& \frac{1}{2} \sum_{q=0}^{M-1} \sum_{l=0}^{L-1} \ln\left(2\pi\sigma^2_{q,l}(u)\right) \\ &+ \sum_{q=0}^{M-1} \sum_{l=0}^{L-1} \frac{(r_{q,l}(u) - \mu_{q,l}(u))^2}{\sigma^2_{q,l}(u)} \end{aligned} \tag{20}$$

From the above analysis, we can see that the SAML detector has the complexity of $O(M^k)$. Hence, it is only practical for application, when the number of nano-machines is relatively small and when the value of M is not big.

G. Complexity of Detection Schemes

Now we analyze the complexity of the detection schemes considered above. In order to describe the complexity of different operations, we assume that the arithmetic operation of individual elements in a matrix has the complexity of $\mathcal{O}(1)$. Since some detection algorithms are joint multiuser detectors, for convenience of comparison, the complexity is expressed in terms of K symbols simultaneously transmitted by K nano-machines.

Let us first analyze the complexity of TMVD. First, its threshold-based decision operation has the complexity of $\mathcal{O}(ML)$, as all the $(M \times L)$ elements in $\boldsymbol{R}_u$ need to be compared with the threshold. Assume that after the threshold-based decision operations, there are Q_a out of the ML elements marked. Then, de-spreading these elements by invoking K MTS codes requires the total complexity of $\mathcal{O}(KQ_a)$. Finally, the majority voting requires $\mathcal{O}(K(L-1)M)$ additions to count the numbers of entries activated in the M rows and $\mathcal{O}(K(M-1))$ comparisons to identify the majority rows. Hence, the total complexity of TMVD is $\mathcal{O}(ML+K(Q_a+ML-1))$. Having obtained the complexity of TMVD, the TMVD-MDDIC can be analyzed as follows. For the analysis, we assume that the numbers of candidate rows in de-spread matrices $\{\boldsymbol{D}_1, \ldots, \boldsymbol{D}_K\}$ are $\{Q_b^{(1)}, \ldots, Q_b^{(K)}\}$. Then, the number of possible combinations N_{MDD} in Section III-B is $N_{MDD} = \prod_{k=1}^{K} Q_b^{(k)}$, meaning that there are N_{MDD} iterations. In every iteration, the complexity of re-spreading the candidate symbols is $\mathcal{O}(KL)$ and also, there are in total $ML(K-1)$ logical OR additions for processing $\boldsymbol{E}_{ik}$. To obtain the Hamming distance between $\boldsymbol{R}_T$ and $\boldsymbol{F}_i$, the complexity is $\mathcal{O}(2ML-1)$ in an iteration. After the iterations, the complexity for the comparisons to select the most likely combination is $\mathcal{O}(N_{MDD}-1)$. After considering all the above operations, the complexity of MDDIC can be found to be $\mathcal{O}(N_{MDD}L(K+MK+M)-1)$. With the complexity of TMVD, the complexity of TMVD-IIC can also be straightforwardly analyzed. As the complexity of TMVD-IIC is related to the number of symbols detected in every iteration, which is uncertain, we instead analyze the complexity upper-bound of the TMVD-IIC. Note that, from our simulations, we find that, typically, three iterations are sufficient. When all the candidate rows are considered in each iteration, it can be shown that the complexity upper-bound is about $\mathcal{O}(2LK^2+(Q_a+ML+L-1)K+ML+3L(Q_b^{(1)}+\ldots+Q_b^{(K)}))$. However, we should

TABLE I
COMPLEXITY OF POST-PROCESSING AND THAT OF DETECTION FOR VARIOUS DETECTION SCHEMES.

Detector	Complexity
TMVD	$\mathcal{O}(ML + K(Q_a + ML - 1))$
TMVD-MDDIC	$\mathcal{O}(K(Q_a + ML - 1) + N_{MDD}L(K + MK + M) + ML - 1)$
TMVD-IIC (upper bond)	$\mathcal{O}(2LK^2 + (Q_a + ML + L - 1)K + ML + 3L(Q_b^{(1)} + \ldots + Q_b^{(K)}))$
EGCD	$\mathcal{O}(K(2ML - M - L))$
EGCD-NIIC	$\mathcal{O}(N_{NIIC}[(\frac{2K+1-N_{NIIC}}{2})(M^2 + 2ML - 4M + 4) - 2ML + M + 2L - 1] + K(2ML - M - L))$
SAML	$\mathcal{O}(M^K(L + 3ML + KI + 1))$

note that the real computation required is much lower than this bound, as the symbols detected in the previous iterations are not required to be considered in the following iterations.

The complexity of EGCD can be readily derived, which is $\mathcal{O}(K(2ML - M - L))$. To analyze the complexity of EGCD-NIIC, we first calculate the complexity of the NIIC invoked. When given N_{NIIC} iterations for detecting the N_{NIIC} most reliable nano-machines, according to Algorithm 3, the complexity of each iteration can be analyzed step-by-step as follows. 1) The de-spreading invoking $(K - j + 1)$ nano-machines' signature codes costs $\mathcal{O}((K - j + 1)ML)$ $j = 1, 2, \ldots, N_{NIIC}$ of computations. 2) The complexity of EGC on the de-spread matrices is $\mathcal{O}(M(L-1)(K-j+1))$. 3) The measurement of $(K - j + 1)$ nano-machines' reliabilities requires the complexity of $\mathcal{O}([((M-1)(M-2)+1](K-j+1))$. 4) The complexity of finding the most reliable nano-machine is $\mathcal{O}(K-j)$. 5) The erasure operation of the L entries activated by the most reliable nano-machine requires the complexity of $\mathcal{O}(L)$. Therefore, the total complexity of N_{NIIC} iterations is $\mathcal{O}(N_{NIIC}[(\frac{2K+1-N_{NIIC}}{2})(M^2 + 2ML - 4M + 4) + L - 1])$. Then, the detection of the symbols sent by the rest $K - N_{NIIC}$ nano-machines requires $\mathcal{O}((K - N_{NIIC})(2ML - M - L))$ calculations. Consequently, the overall complexity of EGCD-NIIC is $\mathcal{O}(N_{NIIC}[(\frac{2K+1-N_{NIIC}}{2})(M^2 + 2ML - 4M + 4) - 2ML + M + 2L - 1] + K(2ML - M - L))$.

Finally, the complexity of SAML can be analyzed as follows. First, spreading the M^K possible combinations of symbols sent by K nano-machines requires the complexity of $\mathcal{O}(M^K L)$. Then, to obtain the means and variances of the received signals of all the possible combinations, the complexity is $\mathcal{O}(M^K KI)$, where I is the ISI length considered. Finally, the complexity for decision-making is approximately $\mathcal{O}(M^K(3ML + 1))$. Hence, the overall complexity of SAML is $\mathcal{O}(M^K(L + 3ML + KI + 1))$.

The complexities of all the considered detection schemes are summarized in Table I. Explicitly, provided that $K \geq 3$, SAML has the highest complexity followed by the TMVD-MDDIC, whose complexity is related to $N_{MDD} = \prod_{k=1}^{K} Q_b^{(k)}$. The value of N_{MDD} can be a big value if the threshold in TMVD is set to be a low value. On the contrary, if the threshold in TMVD is relatively big, N_{MDD} can be small. In practice, the threshold should be appropriately set to make both the false-alarm and miss probabilities sufficiently small. Subsequently, EGCD-NIIC has a higher complexity than TMVD-IIC, as TMVD-IIC can usually complete the detection in three iterations. Fundamentally, TMVD has the lowest complexity followed by EGCD having a slightly higher complexity than TMVD.

IV. PERFORMANCE RESULTS AND DISCUSSION

In this section, the error performance of the MTS-MoSK DMC systems with respectively the TMVD, TMVD-IIC, MD-DIC, EGCD, EGCD-NIIC and SAML is demonstrated against the signal-to-noise ratio (SNR) per bit, SNR_b, in the context of some cases. The performance results were obtained from the Monte-Carlo simulations with random data generated by statistical models. To carry out a fair comparison between different settings, we consider the error performance against SNR_b. Following [51], SNR_b is defined as the ratio between the power (number of molecules) received from a pulse of molecules emitted for transmitting one isolated bit and the corresponding noise power. Assume that within the observation space with a volume V, the expected concentration at the sampling time is $c_{b(o)}$. Then, according to [42], the number of molecules presenting in the observation space follows the Poisson distribution with the mean and variance both given by $Vc_{b(o)}$. Hence, the SNR_b is

$$\text{SNR}_b = \frac{(Vc_{b(o)})^2}{Vc_{b(o)}} = Vc_{b(o)}. \tag{21}$$

Based on the above definition, when given SNR_b and volume V, we can obtain $c_{b(o)}$ from (21). If the communication distance r_k between a nano-machine and AP is known, according to (2), the number of molecules A_b for transmitting one bit can be calculated. As in MTS-MoSK DMC systems, each symbol conveys $b = \log_2 M$ bits, the total number of molecules emitted for transmitting one symbol is $A_s = b \times A_b$. On the other side, due to the introduction of MTS, the transmission of a symbol is split into L chips to transmit L pulses of molecules. Hence, the number of molecules emitted by each chip pulse is $A_h = A_s/L = b \times A_b/L$.

In our demonstration of performance result, unless specifically stated, some of the parameters in our simulations are fixed, which include $D = 2.2 \times 10^{-9}$ m^2/s and $V = 4\pi\rho^3/3$ with $\rho = 20$ nm. The duration of one bit is set to $T_b = 6 \times 10^{-5}$ s, so one symbol duration is $T_s = b \times (6 \times 10^{-5})$ s. Moreover, to take the effect of ISI into consideration, we evaluate the effective length of a transmitted molecular pulse according to

$$I \triangleq \arg_i \left\{ \frac{c_{h(i)}}{c_{h(o)}} \leq 0.1\% \right\} \tag{22}$$

where $c_{h(o)}$ in (22) is the maximun concentration expected within the first chip's duration, when a molecular pulse is started transmitting at $t = 0$, and $c_h(i)$ is the residue concentration of this molecular pulse sampled at the ith chip-duration. From (22) we are implied that only the residue concentration in the following chip-durations with the strength above 0.1% of the peak concentration in the initial chip-duration is counted. Additionally, we assume the random MTS codes in all simulations.

A. Impact of Threshold on the Performance of TMVD

Let us first demonstrate the effect of the normalized threshold α, seen in (7), on the performance of TMVD. Fig. 6 demonstrates that the probabilities of error, false-alarm and

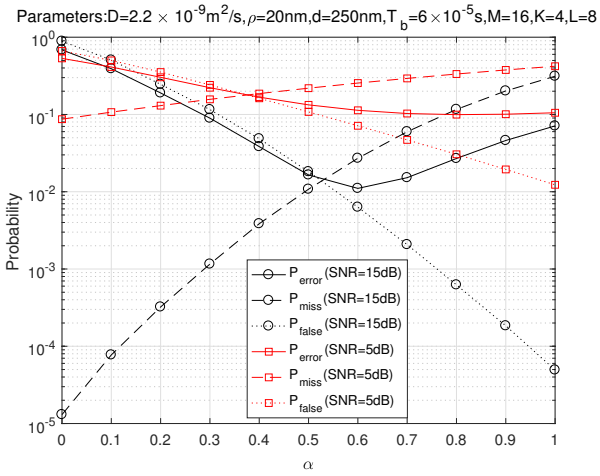

Fig. 6. Probability of error, miss and false-alarm versus α performance of MTS-MoSK DMC systems detected by TMVD with different SNR.

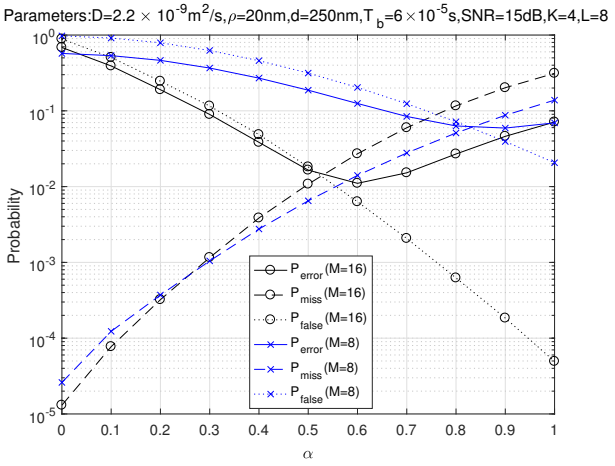

Fig. 7. Probability of error, miss and false-alarm versus α performance of MTS-MoSK DMC systems detected by TMVD.

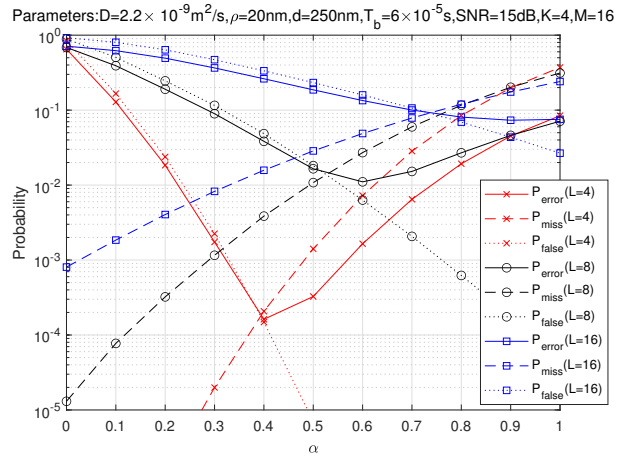

Fig. 8. Probability of error, miss and false-alarm versus α performance of MTS-MoSK DMC systems detected by TMVD, when different number of chips per symbol duration is considered.

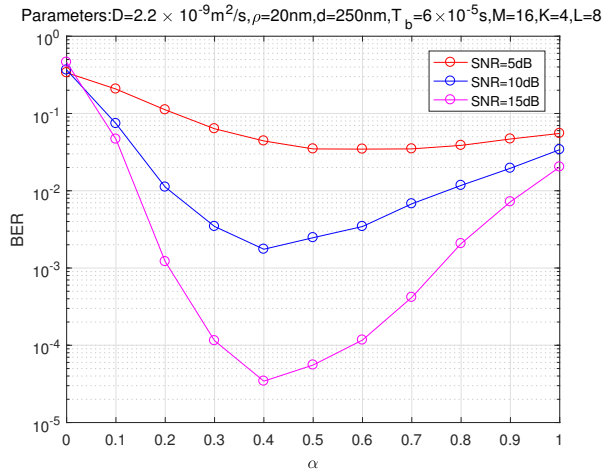

Fig. 9. BER versus α performance of MTS-MoSK DMC systems detected by TMVD, when different SNRs are considered.

miss of TMVD vary with the normalized threshold α, as seen in (7), when SNR$=15dB$ or $5dB$. We can see that as the threshold increases, the probability of false-alarm decreases while that of miss increases. Therefore, a trade-off exists between the probabilities of false-alarm and miss. As shown in Fig. 6, if the general error probability is considered, there is an optimum value for α, which results in that the MTS-MoSK DMC system achieves the lowest error probability. Furthermore, as SNR increases from $5dB$ to $15dB$, the optimum threshold reduces. However, we should note that the optimum threshold is dependent on SNR and is usually hard to derive an analytical solution.

In Fig. 7, we show the probabilities of error, false-alarm and miss of TMVD versus the normalized threshold α, when $M = 16$ and 8 types of molecules are respectively employed. From Fig. 7 we can observe that the miss probability typically reduces and the false probability increases significantly as the number of molecular types employed decreases from $M = 16$ to $M = 8$. The reason behind is that the reduction of M results in severer ISI and MAI, which enhances the molecular concentration around AP. Therefore, the miss probability reduces while the false-alarm probability increases. Again, if the general error probability is considered, there is an optimum value of α that is M-dependent, which makes the error probability minimum.

Fig. 8 illustrates the probabilities of error, false-alarm and miss of TMVD, when $L = 16$, 8 or 4 chips per symbol duration are used. Fig. 8 shows that for the general error probability, the optimum α value is shifted to right as L increases. Furthermore, as L increases, the minimum error probability increases. This is because transmitting more pulses yields higher interference, making the performance of TMVD degrade.

Below we specifically consider BER. First, Fig. 9 shows that the optimum normalized threshold α is around 0.4 in a MTS-MoSK DMC system that employs $M = 16$ types of molecules and $L = 8$ chips per symbol for supporting $K = 4$ nano-machines, wherever the SNR is $10dB$ or $15dB$. The reason behind the above observations is that the normalized threshold α is proportional to the maximum concentration of

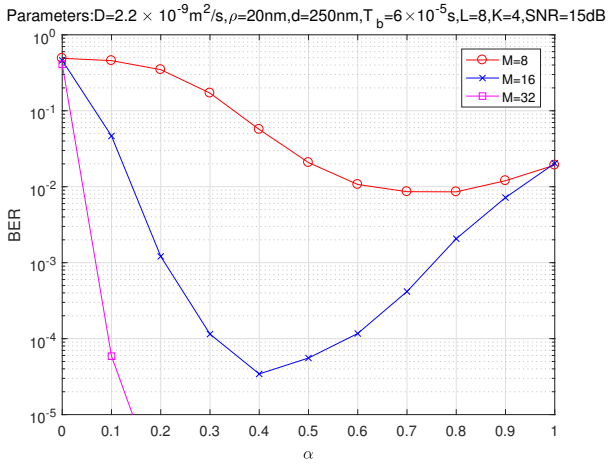

Fig. 10. BER versus α performance of MTS-MoSK DMC systems detected by TMVD, when different numbers of molecular types M are employed.

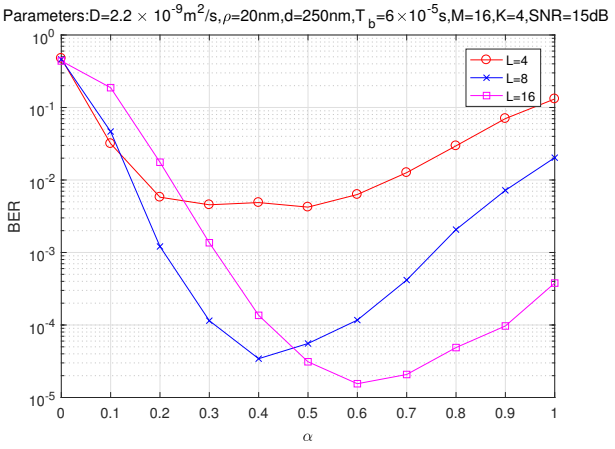

Fig. 11. BER versus α performance of MTS-MoSK DMC systems detected by TMVD, when different length of chips L per symbol duration are considered.

a molecular pulse. Therefore, to demonstrate the performance of the MDDIC and IIC that are based on TMVD, later, the normalized coefficient α is set to 0.5 in our simulations.

In Fig. 10, the optimum normalized threshold α is shifted to left as the number of molecular types increases. This is because for given K and L, the increase of molecular types leads to the reduced MAI and ISI, due to the reduction of concentration at AP. Therefore, when the DMC system employs the larger number, such as $M = 32$, of molecular types to transmit information, the miss probability dominates the error performance and hence the normalized threshold reduces.

Fig. 11 demonstrates the impact of the number of chips per symbol on the bit error performance of the MTS-MoSK DMC systems detected by TMVD. It can be observed that when using more chips per symbol, the optimum normalized threshold α is shifted to right. This is because when L increases, ISI increases as the result of the increased concentration at AP. In this case, the false-alarm becomes dominant of the error performance.

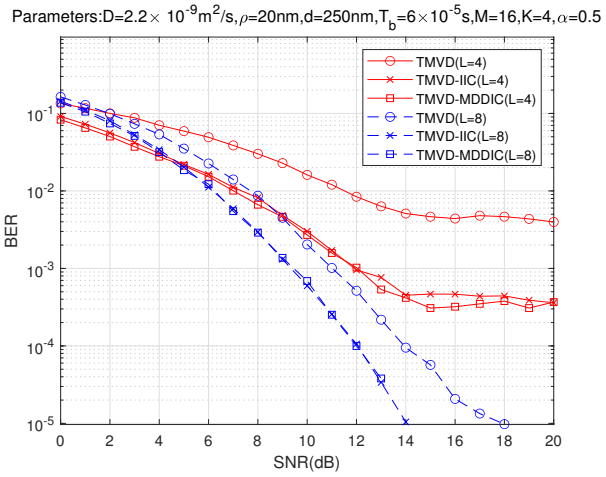

Fig. 12. Comparison of BER versus SNR performance of MTS-MoSK DMC systems detected by TMVD, TMVD-IIC and TMVD-MDDIC, when different L is considered.

B. Performance Comparison of MTS-MoSK DMC Systems with Various Detection Schemes

Let us now compare the error performance of the MTS-MoSK DMC systems with the various detection schemes introduced in this paper. First, Fig. 12 compares the BER performance of the MTS-MoSK DMC systems with TMVD, TMVD-IIC and TMVD-MDDIC, when the different numbers of chips per symbol are considered. From the results of Fig. 12, we observe that in comparison with TMVD, both the interference cancellation assisted methods are capable of improving the bit error performance of the MTS-MoSK DMC systems. This is more significant, when L is small. When compared to TMVD-IIC, TMVD-MDDIC only has a very slight improvement on the BER performance. Hence, when taking both the computation complexity and communication reliability into account, TMVD-IIC is more desirable for application. Additionally, as Fig. 12 shows, the BER performance improves as L is increased from $L = 4$ to $L = 8$, when SNR is sufficiently high. This is because, increasing the value of L can bring more diversity to the detection, which helps to average out the noise and ISI effect.

Fig. 13 illustrates the BER versus SNR performance of the MTS-MoSK DMC systems employing TMVD, TMVD-IIC and TMVD-MDDIC, when different numbers of molecular types, i.e., M, are employed. Explicitly, increasing the value of M results in significant improvement of BER performance for all the detection schemes considered, owing to the fact that MAI and ISI decreases with the increase of M.

In Fig. 14, we compare the BER performance of the MTS-MoSK DMC systems with TMVD, TMVD-IIC and TMVD-MDDIC, when the systems support different numbers of nano-machines. As Fig. 14 shows, when the number of nano-machines increases, yielding the increasing MAI, the BER performance of MTS-MoSK DMC systems degrades. The results also show that when multiple nano-machines are supported, both TMVD-MDDIC and TMVD-IIC have a similar efficiency and achieve similar BER performance, which is much better than the BER performance attained by TMVD. Therefore, both TMVD-MDDIC and TMVD-IIC are efficient for MAI

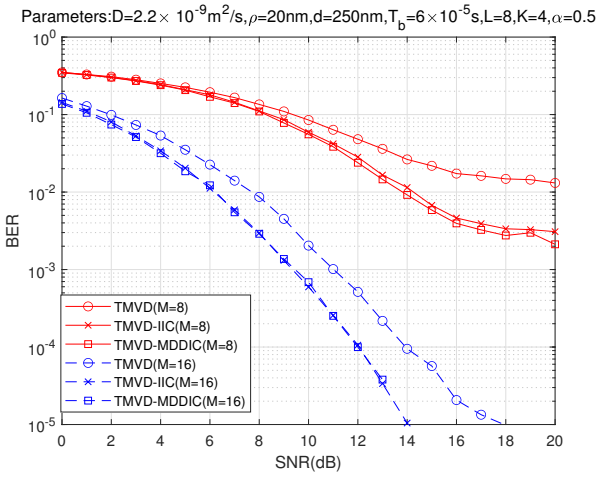

Fig. 13. Comparison of BER versus SNR performance of the MTS-MoSK DMC systems detected by TMVD, TMVD-IIC and TMVD-MDDIC detection schemes, when different numbers of molecular types are employed.

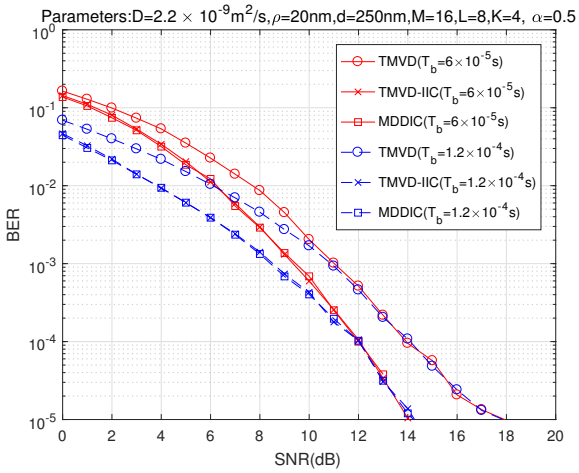

Fig. 15. Comparison of BER versus SNR performance of the MTS-MoSK DMC systems employing TMVD, TMVD-IIC and TMVD-MDDIC, when transmitting at different bit rates of $1/T_b$.

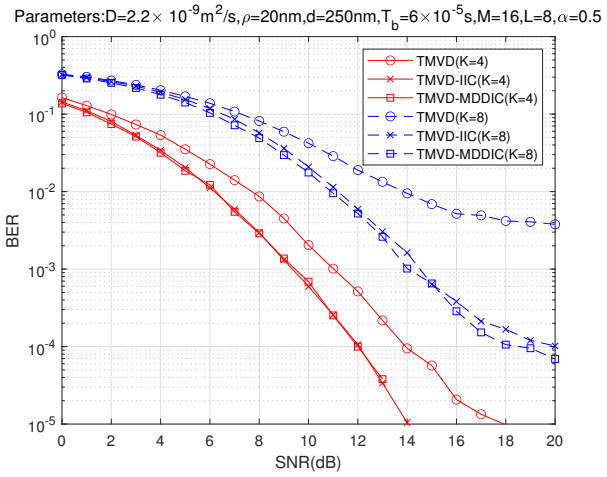

Fig. 14. Comparison of BER versus SNR performance of the MTS-MoSK DMC systems detected by TMVD, TMVD-IIC and TMVD-MDDIC, when different numbers of nano-machines are supported.

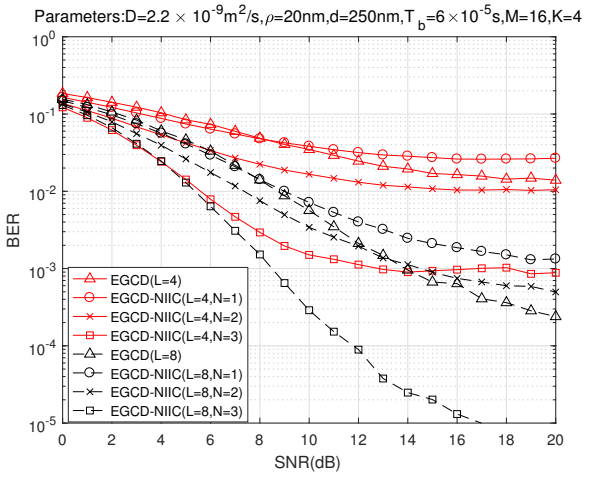

Fig. 16. Comparison of BER versus SNR performance of the MTS-MoSK DMC systems detected by EGCD and EGCD-NIIC, when different values of L are considered.

mitigation, especially, in the relatively high SNR region, where MAI dominates the BER performance.

Fig. 15 shows the transmission rate on the BER performance of the MTS-MoSK DMC systems with TMVD, TMVD-IIC and TMVD-MDDIC. Here, the bit rate is given by $R_b = 1/T_b$ and hence, a higher data rate corresponds to a lower value of T_b. Therefore, as shown in Fig. 15, when the bit rate reduces, the BER performance improves, especially, when SNR is low, which is due to the reduction of ISI, when T_b increases. By contrast, when SNR increases, the performance attained in two cases converge. This is because the threshold applied in TMVD is adjusted according to the bit interval. When SNR is high, the error performance of TMVD is insensitive to the bit rate, provided that it satisfies the assumption for sampling stated in Section II-B.

In Fig. 16, the BER performance of MTS-MoSK DMC systems detected by EGCD and EGCD-NIIC is compared, when different length of chips L per symbol duration are considered. Furthermore, for the EGCD-NIIC, the impact of the number of iterations for IIC, i.e. N, on the achievable BER performance is investigated. As Fig. 16 shows, the error performance for both L values improves as the value of N increases. It can be expected that the best BER performance is achieved in the case of $N = K-1$. However, increasing the number of iterations of IIC results in the increase of detection complexity. Hence, the EGCD-NIIC detection scheme can provide a trade-off between BER performance and detection complexity. Additionally, as seen in Fig. 16, in both cases, the EGCD-NIIC with $N = 1$ achieves worse BER performance than the EGCD, when SNR is relatively high. The reason for the observation is that the EGCD-NIIC is more efficient, when signals appear more like Gaussian signals. When SNR is high, interference dominates, making the EGCD-NIIC less efficient. This is also the reason that in Fig. 16 the BER curves with $N \geq 1$ present error floors, when SNR is high.

Fig. 17 compares the BER performance of the MTS-MoSK DMC systems detected by EGCD and EGCD-NIIC with respect to different values of M. Explicitly, when the value

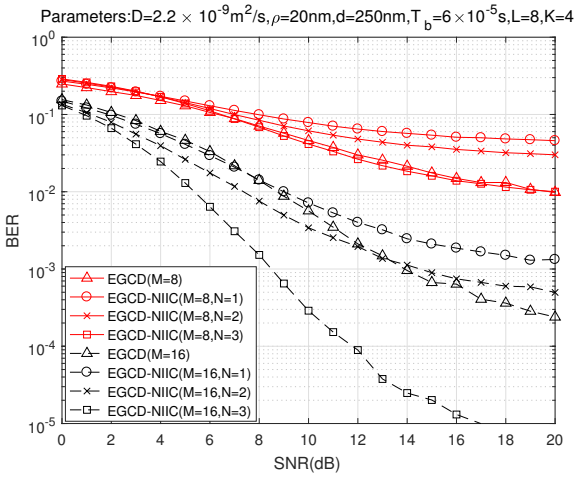

Fig. 17. Comparison of BER versus SNR performance of the MTS-MoSK DMC systems employing EGCD and EGCD-NIIC, when different numbers of molecular types M are employed.

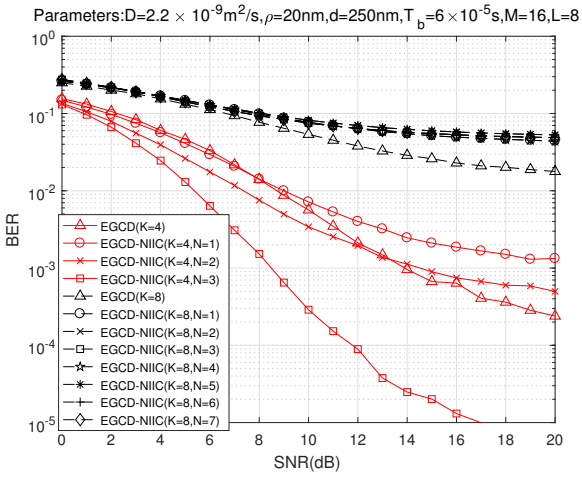

Fig. 18. Comparison of BER versus SNR performance of the MTS-MoSK DMC systems employing EGCD and EGCD-NIIC, when different number of nano-machines is supported.

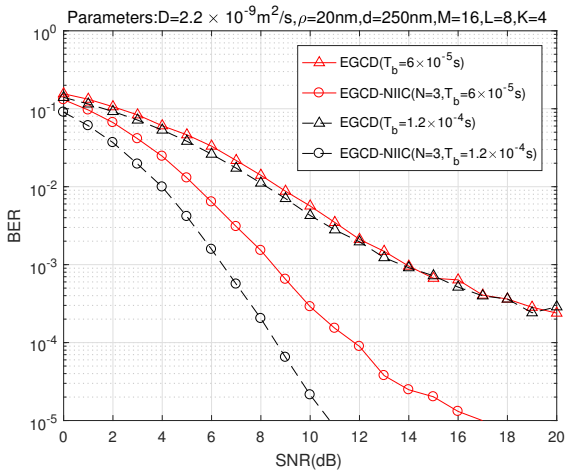

Fig. 19. Comparison of BER versus SNR performance of the MTS-MoSK DMC systems employing EGCD and EGCD-NIIC, when different bit rate of $1/T_b$ is transmitted.

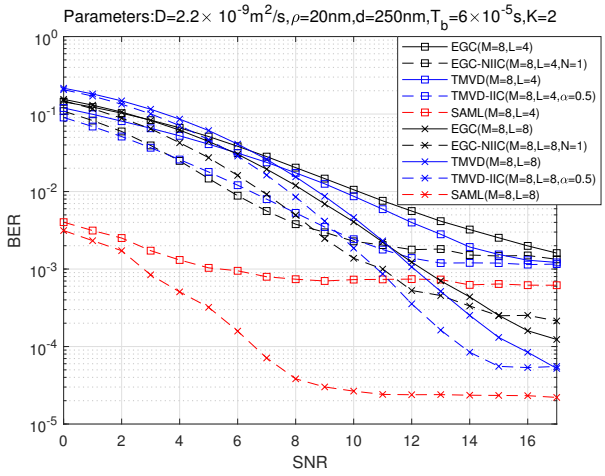

Fig. 20. Comparison of BER versus SNR performance of the MTS-MoSK DMC systems employing EGCD, EGCD-NIIC, TMVD, TMVD-IIC and SAML, when different values of L are considered.

of M increases, the BER performance attained by both the detection schemes significantly improve. Furthermore, for a given SNR, the EGCD-NIIC with a sufficient number of IIC stages can significantly outperform the EGCD without the attempt of interference mitigation.

In Fig. 18, we compare the BER performance of the MTS-MoSK DMC systems employing EGCD and EGCD-NIIC, when the systems support different numbers of nano-machines associated with using different numbers of iterations in the NIIC. It is shown that when K is too big ($K = 8$), the application of NIIC is unable to gain any performance improvement. This is because when K is large resulting in high interference, the reliability measurement by (12) is unable to identify the most reliable nano-machine. In this case, interference cancellation in fact introduces extra interference, which results in performance degradation. Therefore, by also considering the results in Fig. 17, we can know that the EGCD-NIIC scheme requires a relatively high budget of M/K to gain the benefit of performance improvement.

The BER performance of the MTS-MoSK DMC systems employing respectively EGCD and EGCD-NIIC to support different transmission rates is compared in Fig. 19. As the results of Fig. 19 show, for the two bit rates considered, EGCD achieves nearly the same BER performance. By contrast, when the EGCD-NIIC with $N = 3$ is employed, significant performance improvement is observed, when the bit rate is reduced from about 16.7K to about 3.3K. Therefore, when the symbol duration becomes longer, resulting the reduction of ISI, the interference cancellation in the EGCD-NIIC becomes more efficient and hence, the BER performance improves.

In Fig. 20, we compare the BER performance of the MTS-MoSK DMC systems employing the various detection schemes introduced in this paper, when $K = 2$ nano-machines are supported. In addition to the detection schemes considered in the previous figures, explicitly, the SAML detector achieves the best BER performance, while at the cost of the highest detection complexity. Furthermore, we can observe that even

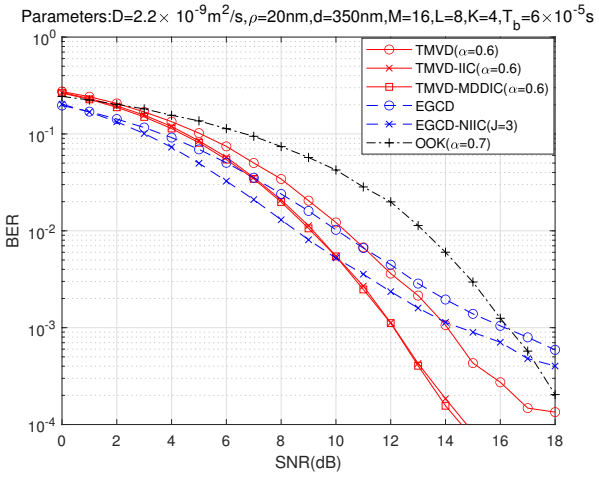

Fig. 21. Comparison of the BER versus SNR performance of the MTS-MoSK DMC systems employing the TMVD-series or EGCD-series of detection schemes and that of the MDMA DMC system employing OOK.

for the SAML, the BER curves appear error floors in high SNR region. The reason behind is that the SAML assumes that all the previously detected symbols are correct, which is practically not true. Therefore, when there are erroneously detected symbols, they impose interference on the following detections but the SAML detector ignores and hence, it results in error floor.

C. Comparison of MTS-MoSK DMC System with MDMA DMC System

Above the BER performance of the MTS-MoSK DMC systems employing various detection schemes has been demonstrated and compared. Finally, in Fig. 21, we compare the BRE performance of our MTS-MoSK DMC systems employing respectively the TMVD-series and EGCD-series of detection schemes with that of the legacy MDMA DMC [19–25] system employing OOK modulation. As mentioned in Section I, MDMA DMC scheme assigns unique types of molecules to support the signal transmissions of different nano-machines. Hence, there is no MAI in MDMA DMC systems. For fair comparison, we assume the same bit rate $R_b = 1/T_b = 1/6 \times 10^{-5}$ and the same SNR per-bit budget. All parameters used in individual detectors are set to the nearly optimal values, including that the activation threshold of $0.6c_h(0)$ in TMVD-series of detectors, 3 iterations of EGCD-NIIC, and the decision threshold of $0.7c_b(0)$ in OOK demodulation. As shown in Fig. 21, within the BER range $(10^{-2}, 10^{-3})$ of practically interest, all the MTS-MoSK DMC schemes outperform the OOK-based MDMA scheme. The main reason behind is that the OOK-based MDMA DMC experiences severe ISI. By contrast, the MTS-MoSK DMC is capable of efficiently mitigating ISI via molecular type hopping and MoSK modulation. As shown in Fig. 21, when the SNR is very high, such as higher than 16 dB or 17 dB, the MTS-MoSK DMC with the EGCD-series of detectors may be outperformed by the OOK-based MDMA DMC. Nevertheless, in practice, the schemes performing well in relatively low SNR are usually desired, as above-mentioned.

V. Conclusions

This paper has focused on comparing the performance of the MTS-MoSK DMC systems with various detection schemes, which include three proposed interference cancellation relied schemes, namely, TMVD-IIC, TMVD-MDDIC and EGCD-NIIC, a proposed SAML detector, and two legacy single-user detection schemes, namely TMVD and EGCD. The impacts of the various parameters involved in system design, signal propagation and detector design have been comprehensively investigated and demonstrated via simulations. The studies and performance results show that both TMVD-IIC and TMVD-MDDIC are efficient to mitigate MAI and achieve the similar BER performance, which is much better than that attainable by TMVD and EGCD. In particular, TMVD-IIC has the advantage of a lower complexity than TMVD-MDDIC. When a proper number, i.e., N, is used for interference cancellation, EGCD-NIIC can significantly outperform EGCD. However, the complexity of EGCD-NIIC increases with N, but a very small value of N yields limited performance gain. Among the detection schemes considered, SAML is capable of achieving the best error performance, but it also has the impractically high complexity. Therefore, when the performance-complexity trade-off is concerned, TMVD-IIC is the most promising detection scheme for the MTS-MoSK DMC systems. Our future work will be extended to study the efficient interference cancellation schemes in the MTS-MoSK DMC systems where transmit nano-machines have certain mobility.

References

[1] I. F. Akyildiz, M. Pierobon, S. Balasubramaniam, and Y. Koucheryavy, "The internet of bio-nano things," *IEEE Communications Magazine*, vol. 53, no. 3, pp. 32–40, 2015.

[2] B. Atakan, O. B. Akan, and S. Balasubramaniam, "Body area nanonetworks with molecular communications in nanomedicine," *IEEE Communications Magazine*, vol. 50, no. 1, pp. 28–34, 2012.

[3] M. Kuscu and O. B. Akan, "The internet of molecular things based on fret," *IEEE Internet of Things Journal*, vol. 3, no. 1, pp. 4–17, 2016.

[4] W. Gao, T. Mak, and L.-L. Yang, "Type-spread molecular communications: Principles and inter-symbol interference mitigation," in *ICC 2019 - 2019 IEEE International Conference on Communications (ICC)*, 2019, pp. 1–6.

[5] L. Felicetti, M. Femminella, and G. Reali, "A molecular communications system for live detection of hyperviscosity syndrome," *IEEE Transactions on NanoBioscience*, vol. 19, no. 3, pp. 410–421, 2020.

[6] S. Ghavami, "Anomaly detection in molecular communications with applications to health monitoring networks," *IEEE Transactions on Molecular, Biological and Multi-Scale Communications*, vol. 6, no. 1, pp. 50–59, 2020.

[7] T. Nakano, Y. Okaie, S. Kobayashi, T. Hara, Y. Hiraoka, and T. Haraguchi, "Methods and applications of mobile molecular communication," *Proceedings of the IEEE*, vol. 107, no. 7, pp. 1442–1456, 2019.

[8] X. Chen, M. Wen, F. Ji, Y. Huang, Y. Tang, and A. W. Eckford, "Detection interval of aerosol propagation from the perspective of molecular communication: How long is enough?" *IEEE Journal on Selected Areas in Communications*, vol. 40, no. 11, pp. 3255–3270, 2022.

[9] Y. Huang, F. Ji, M. Wen, X. Chen, Y. Tang, and B. Zheng, "Survey on macro-scale molecular communication prototypes," *SCIENTIA SINICA Informationis*, vol. 51, no. 12, pp. 2016–2036, 2021.

[10] Y. Tang, Y. Huang, C.-B. Chae, W. Duan, M. Wen, and L.-L. Yang, "Molecular-type permutation shift keying in molecular mimo communications for iobnt," *IEEE Internet of Things Journal*, vol. 8, no. 21, pp. 16 023–16 034, 2021.

[11] Y. Tang, M. Wen, X. Chen, Y. Huang, and L.-L. Yang, "Molecular type permutation shift keying for molecular communication," *IEEE Transactions on Molecular, Biological and Multi-Scale Communications*, vol. 6, no. 2, pp. 160–164, 2020.

[12] Y. Tang, F. Ji, M. Wen, Q. Wang, and L.-L. Yang, "Enhanced molecular type permutation shift keying for molecular communication," *IEEE Wireless Communications Letters*, vol. 10, no. 12, pp. 2722–2726, 2021.

[13] X. Chen, Y. Huang, L.-L. Yang, and M. Wen, "Generalized molecular-shift keying (gmosk): Principles and performance analysis," *IEEE Transactions on Molecular, Biological and Multi-Scale Communications*, vol. 6, no. 3, pp. 168–183, 2020.

[14] Y. Huang, F. Ji, Z. Wei, M. Wen, X. Chen, Y. Tang, and W. Guo, "Frequency domain analysis and equalization for molecular communication," *IEEE Transactions on Signal Processing*, vol. 69, pp. 1952–1967, 2021.

[15] L. Shi and L.-L. Yang, "Equalisation and performance of diffusive molecular communication systems with binary molecular-shift keying modulation," *IET Communications*, vol. 14, no. 4, pp. 549–555, 2020.

[16] T. N. Cao, V. Jamali, N. Zlatanov, P. L. Yeoh, J. Evans, and R. Schober, "Fractionally spaced equalization and decision feedback sequence detection for diffusive mc," *IEEE Communications Letters*, vol. 25, no. 1, pp. 117–121, 2021.

[17] V. Jamali, N. Farsad, R. Schober, and A. Goldsmith, "Non-coherent detection for diffusive molecular communication systems," *IEEE Transactions on Communications*, vol. 66, no. 6, pp. 2515–2531, 2018.

[18] Z. Wei, W. Guo, B. Li, J. Charmet, and C. Zhao, "High-dimensional metric combining for non-coherent molecular signal detection," *IEEE Transactions on Communications*, vol. 68, no. 3, pp. 1479–1493, 2020.

[19] L. Parcerisa Giné and I. F. Akyildiz, "Molecular communication options for long range nanonetworks," *Computer Networks*, vol. 53, no. 16, pp. 2753–2766, 2009. [Online]. Available: https://www.sciencedirect.com/science/article/pii/S1389128609002540

[20] X. Chen, M. Wen, C.-B. Chae, L.-L. Yang, F. Ji, and K. K. Igorevich, "Resource allocation for multiuser molecular communication systems oriented to the internet of medical things," *IEEE Internet of Things Journal*, vol. 8, no. 21, pp. 15 939–15 952, 2021.

[21] G. Aminian, M. Farahnak-Ghazani, M. Mirmohseni, M. Nasiri-Kenari, and F. Fekri, "On the capacity of point-to-point and multiple-access molecular communications with ligand-receptors," *IEEE Transactions on Molecular, Biological and Multi-Scale Communications*, vol. 1, no. 4, pp. 331–346, Dec 2015.

[22] A. Ghasempour, "Using a genetic-based algorithm to solve the scheduling optimization problem for long-range molecular communications in nanonetworks," in *2015 IEEE 26th Annual International Symposium on Personal, Indoor, and Mobile Radio Communications (PIMRC)*, 2015, pp. 1825–1829.

[23] N. Farsad, H. B. Yilmaz, C.-B. Chae, and A. Goldsmith, "Energy model for vesicle-based active transport molecular communication," in *2016 IEEE International Conference on Communications (ICC)*, 2016, pp. 1–6.

[24] B. Atakan and O. B. Akan, "Single and multiple-access channel capacity in molecular nanonetworks," in *International Conference on Nano-Networks*. Springer, 2009, pp. 14–23.

[25] M. C. Gursoy, A. E. Pusane, and T. Tugcu, "Molecule-as-a-frame: A frame based communication approach for nanonetworks," *Nano Commun. Networks*, vol. 16, pp. 45–59, 2018.

[26] Y. Zamiri-Jafarian, S. Gazor, and H. Zamiri-Jafarian, "Molecular code division multiple access in nano communication systems," in *2016 IEEE Wireless Communications and Networking Conference*, April 2016, pp. 1–6.

[27] L. Wang and A. W. Eckford, "Nonnegative code division multiple access techniques in molecular communication," in *2017 15th Canadian Workshop on Information Theory (CWIT)*, June 2017, pp. 1–5.

[28] S. Korte, M. Damrath, M. Damrath, and P. A. Hoeher, "Multiple channel access techniques for diffusion-based molecular communications," in *SCC 2017; 11th International ITG Conference on Systems, Communications and Coding*, Feb 2017, pp. 1–6.

[29] H. Tezcan, S. Oktug, and F. N. Kok, "Neural delay lines for tdma based molecular communication in neural networks," in *2012 IEEE International Conference on Communications (ICC)*, June 2012, pp. 6209–6213.

[30] R. Yu, M. S. Leeson, and M. D. Higgins, "Multiple-access scheme optimisation for artificial neuronal networks," in *2014 9th International Symposium on Communication Systems, Networks Digital Sign (CSNDSP)*, July 2014, pp. 428–433.

[31] Y. Okaie, T. Nakano, M. Moore, and J.-Q. Liu, "Information transmission through a multiple access molecular communication channel," in *2013 IEEE International Conference on Communications (ICC)*, 2013, pp. 4030–4034.

[32] M. J. Moore and T. Nakano, "Multiplexing over molecular communication channels from nanomachines to a micro-scale sensor device," in *2012 IEEE Global Communications Conference (GLOBECOM)*, 2012, pp. 4302–4307.

[33] M. Damrath and P. A. Hoeher, "Low-complexity adaptive threshold detection for molecular communication," *IEEE Transactions on NanoBioscience*, vol. 15, no. 3, pp. 200–208, April 2016.

[34] A. Pouttu, H. Saarnisaari, and S. Glisic, "Noncoherent m mcsk-m mfsk modulation in rayleigh fading channel," in *MILCOM 2006 - 2006 IEEE Military Communications conference*, Oct 2006, pp. 1–5.

[35] S. Ahmed, R. G. Maunder, L. Yang, and L. Hanzo, "Iterative detection of unity-rate precoded ffh-mfsk and irregular variable-length coding," *IEEE Transactions on Vehicular Technology*, vol. 58, no. 7, pp. 3765–3770, Sep. 2009.

[36] W. Gao, T. Mak, and L.-L. Yang, "Molecular type spread molecular shift keying for multiple-access diffusive molecular communications," *IEEE Transactions on Molecular, Biological and Multi-Scale Communications*, vol. 7, no. 1, pp. 51–63, 2021.

[37] G. Weidong, M. Terrence, and Y. Lie-liang, "Equal-gain combining with interference mitigation for molecular type hopping assisted molecular shift keying systems," *ITU Journal on Future and Evolving Technologies*, vol. 2, pp. 157–164, 2021.

[38] D. J. Goodman, P. S. Henry, and V. K. Prabhu, "Frequency-hopped multilevel fsk for mobile radio," *The Bell System Technical Journal*, vol. 59, no. 7, pp. 1257–1275, Sept 1980.

[39] N. Kim and C. Chae, "Novel modulation techniques using isomers as messenger molecules for nano communication networks via diffusion," *IEEE Journal on Selected Areas in Communications*, vol. 31, no. 12, pp. 847–856, 2013.

[40] L. Shi and L. Yang, "Diffusion-based molecular communications: Inter-symbol interference cancellation and system performance," in *2016 IEEE/CIC International Conference on Communications in China (ICCC)*, July 2016, pp. 1–6.

[41] I. Llatser, A. Cabellos-Aparicio, M. Pierobon, and E. Alarcon, "Detection techniques for diffusion-based molecular communication," *IEEE Journal on Selected Areas in Communications*, vol. 31, no. 12, pp. 726–734, December 2013.

[42] M. Pierobon, I. F. Akyildiz *et al.*, "Diffusion-based noise analysis for molecular communication in nanonetworks," *IEEE Transactions on Signal Processing*, vol. 59, no. 6, pp. 2532–2547, 2011.

[43] D. Kilinc and O. B. Akan, "Receiver design for molecular communication," *IEEE Journal on Selected Areas in Communications*, vol. 31, no. 12, pp. 705–714, December 2013.

[44] L. Meng, P. Yeh, K. Chen, and I. F. Akyildiz, "On receiver design for diffusion-based molecular communication," *IEEE Transactions on Signal Processing*, vol. 62, no. 22, pp. 6032–6044, Nov 2014.

[45] M. Pierobon and I. F. Akyildiz, "Diffusion-based noise analysis for molecular communication in nanonetworks," *IEEE Transactions on Signal Processing*, vol. 59, no. 6, pp. 2532–2547, 2011.

[46] D. J. Goodman, P. Henry, and V. Prabhu, "Frequency-hopped multilevel fsk for mobile radio," *The Bell System Technical Journal*, vol. 59, no. 7, pp. 1257–1275, 1980.

[47] U.-C. Fiebig, "Iterative interference cancellation for ffh/mfsk ma systems," *IEE Proceedings-Communications*, vol. 143, no. 6, pp. 380–388, 1996.

[48] L.-L. Yang, *Multicarrier communications*. John Wiley & Sons, 2009.

[49] F. Yang and L.-l. Yang, "Low-complexity noncoherent fusion rules for wireless sensor networks monitoring multiple events," *IEEE Transactions on Aerospace and Electronic Systems*, vol. 50, no. 3, pp. 2343–2353, 2014.

[50] F. Yang and L.-L. Yang, "Frequency-hopping/m-ary frequency-shift keying wireless sensor network monitoring multiple source events," in *2012 IEEE 75th Vehicular Technology Conference (VTC Spring)*, 2012, pp. 1–5.

[51] L. Shi and L. Yang, "Error performance analysis of diffusive molecular communication systems with on-off keying modulation," *IEEE Transactions on Molecular, Biological and Multi-Scale Communications*, pp. 1–1, 2018.